HHS Public Access

Author manuscript

*Nat Neurosci*. Author manuscript; available in PMC 2021 March 03.

Published in final edited form as:

*Nat Neurosci*. 2020 August ; 23(8): 968–980. doi:10.1038/s41593-020-0657-z.

# Anatomic resolution of neurotransmitter-specific projections to the VTA reveals diversity of GABAergic inputs

**Marta E. Soden**[1,2], **Amanda S. Chung**[1,2], **Beatriz Cuevas**[2], **Jesse M. Resnick**[1], **Rajeshwar Awatramani**[3], **Larry S. Zweifel**[1,2]

[1]Department of Psychiatry and Behavioral Sciences, University of Washington, Seattle, 98195.

[2]Department of Pharmacology, University of Washington, Seattle, 98195.

[3]Department of Neurology, Northwestern University, Chicago, IL 60611.

## Abstract

The ventral tegmental area (VTA) is important for reward processing and motivation. The anatomic organization of neurotransmitter-specific inputs to the VTA remains poorly resolved. Here, we mapped the major neurotransmitter projections to the VTA through cell-type specific retrograde and anterograde tracing. We found that glutamatergic inputs arose from a variety of sources and displayed some connectivity biases towards specific VTA cell types. The sources of GABAergic projections were more widespread, displayed a high degree of differential innervation of subregions in the VTA, and were largely biased towards synaptic contact with local GABA neurons. Inactivation of GABA release from the two major sources, locally derived versus distally derived, revealed distinct roles for these projections in behavioral regulation. Optogenetic manipulation of individual distal GABAergic inputs also revealed differential behavioral effects. These results demonstrate that GABAergic projections to the VTA are a major contributor to the regulation and diversification of the structure.

## Introduction

The VTA is a heterogeneous structure comprised of dopamine-, GABA-, and glutamate-producing neurons[1]. Adding to this complexity, neurons within this region have been shown to be multidimensional with respect to the neurotransmitters they can co-release[1]. Anatomically, the VTA can be subdivided into the rostral VTA (VTAR), rostral linear (RLi), caudal linear (CLi), interfascicular (IF), parabrachial pigmented (PBP), and paranigral (PN) regions[1]. In addition, the posterior VTA contains a high density of GABA-producing neurons and has been further delineated as the rostromedial tegmental area (RMTg)[2], or caudal tail of the VTA[3]. The cell types and subdivisions of the VTA have been proposed to

Correspondence: larryz@uw.edu.

Author Contributions

M.E.S., A.S.C., J.M.R., and L.S.Z designed experiments, collected, and analyzed data. M.E.S. and L.S.Z wrote the manuscript. M.E.S., A.S.C., and J.M.R. performed viral injection surgeries. M.E.S. and B.C. performed behavioral analysis. M.E.S. performed slice electrophysiology. Histology and cell counts were performed by M.E.S., A.S.C., B.C., J.M.R. and L.S.Z. L.S.Z generated CAV2-FLEX-ZsGreen. L.S.Z. and M.E.S purified all viral vectors. R.A. provided the $Th^{FlpO}$ mouse line.

Competing Interests

The authors declare no competing interests.

serve different functions[4–7] through distinct input-output relationships[8–11]. However, cell-type specific viral tracing studies have found a surprising lack of overall specificity of inputs onto the different cell types of the VTA[8,10,12,13].

The majority of projections to the VTA have largely been considered to be glutamatergic[14]. In this view, the diversity of glutamatergic inputs, in conjunction with a limited source of local and long-loop inhibitory inputs to the VTA, determines the functional diversity of the outputs[14,15]. However, accumulating evidence suggests such an organization may be oversimplified. Ultra-structural analysis of synapses in the ventral midbrain revealed that symmetrical synapses, largely representing inhibitory synapses, outnumber asymmetrical excitatory synapses nearly 10-fold[16]. Consistent with this, miniature inhibitory postsynaptic currents (mIPSCs) representing synaptic GABA connectivity are nearly 10-times more frequent than miniature excitatory postsynaptic currents onto dopamine neurons[17]. Previous analysis of inputs to the VTA revealed a large number of projection neurons from a variety of anatomical sources that did not co-localize with glutamatergic markers, but the neurotransmitter phenotype of these projection neurons is not clear[15]. Of further note, non-dopamine neurons in the VTA have nearly 3-times more inhibitory synaptic inputs than dopamine neurons[18]. This disparity in synaptic connectivity could reflect a large number of inhibitory connections from local interneurons within the VTA, or from the RMTg. However, analyses of several individual projections to the VTA from other brain regions have found these to be largely GABAergic inputs that synapse predominantly onto GABA neurons[11,19–23]. Whether these observations are representative of the basic organization of inputs to the VTA or are selective exceptions to the rule remains to be established.

In combination with anterograde tracing, synaptic connectivity analysis, and gene inactivation, we find that GABAergic inputs represent the most widespread source of projections to the VTA. These projections largely innervate distinct subregions of the VTA, and nearly all inputs tested synapsed predominantly onto local GABAergic interneurons and weakly onto non-GABA neurons. Glutamatergic inputs are more limited in their sources and are less diversified in their innervation patterns, but different inputs display varying synaptic properties. Through genetic inactivation of functional GABA signaling from neurons originating within the ventral midbrain or projecting to the VTA from distal regions we find that these two sources of inhibitory input differentially innervate dopamine and non-dopamine neurons of the VTA and have distinct roles in reinforcement learning and social behavior. Furthermore, optogenetic activation and inhibition of distal GABA inputs with varying VTA innervation patterns revealed differential effects on reinforcement and social behaviors. Collectively, these data provide new insights into the basic organizational principles of the VTA and represent an anatomical and functional guide for further dissection of dopamine- and GABA-dependent processes.

## Results

### Anatomical organization of neurotransmitter inputs to the VTA

The major neurotransmitter inputs to the VTA are GABA, glutamate, serotonin, and acetylcholine[14]. To establish the sources of these inputs, we utilized the retrogradely transported canine adenoviral vector (CAV2) containing a conditional expression cassette for

the bright fluorescent protein ZsGreen (CAV2-FLEX-ZsGreen)[24]. CAV2-FLEX-ZsGreen was injected into the VTA of six Cre-driver lines: Vgat-Cre (*Slc32a1*; GABA), Vglut1-, Vglut2-, and Vglut3-Cre (*Slc17a7*, *Slc17a6*, and *Slc17a8*; glutamate), ePet1-Cre (*Fev*, serotonin), and *Chat*-Cre (acetylcholine) (Fig. 1a–b; Supplementary Table 1). Retrogradely labelled neurons were quantified every 90 μm throughout the rostral-caudal extent of the brain based on anatomical registration according to an existing brain atlas[25] (Fig. 1b–d).

In total, we identified 29 brain regions that consistently displayed retrograde labeling (Fig. 1c–g and Extended Data Fig. 1). As expected, we identified one serotonergic input from the dorsal raphe nucleus (DRN) and two cholinergic inputs from the laterodorsal tegmental nucleus (LDTg) and the pedunculopontine tegmental nucleus (PPTg) (Fig. 1d and Extended Data Fig. 2). Glutamatergic inputs varied by region depending on the expression of Vglut1 (cortical), Vglut2 (subcortical), or Vglut3 (DRN), as expected (Extended Data Fig. 1). GABAergic inputs derived from 26 of 29 total regions with the only exceptions in the cortex (Fig. 1b–e). Although glutamatergic inputs were derived from a variety of sources (16 of 29, Fig. 1b, c, f, and g), GABAergic inputs outnumbered glutamatergic inputs in many regions (Fig. 1c and Extended Data Fig. 1).

GABAergic neurons were found across the rostral-to-caudal extent of the striatopallidal complex, the extended amygdala, and the hypothalamus (Fig. 1 c, e, and g, and Extended Data Fig. 1). In contrast, glutamatergic inputs were widespread throughout the OFC, mPFC, and Cingulate, and had significant numbers of cells within the hindbrain but displayed relative sparse labeling in other subcortical structures (Fig. 1c, f, and g and Extended Data Fig. 1). We also observed numerous cells labeled in the VTA of Vglut2-Cre (511.8 ± 35.66) and Vgat-Cre mice (713.2 ± 54.61) that displayed some differential rostral-to-caudal location within the VTA (Extended Data Fig. 1). This observation is consistent with the reported local distribution and connectivity of these cell types[6,26,27], with previous estimations of more GABAergic than glutamatergic neurons within the VTA[14], and indicates the relative equivalency of viral transduction of Vglut2- and Vgat-expressing neurons by CAV2. Due to the locations of these neurons within the VTA, they were excluded from the total cell counts and analyses of projections to the VTA (Fig. 1a–g). We observed relatively few infected neurons in the substantia nigra (SN) pars compacta and pars reticulata adjacent to the VTA (Extended Data Fig. 1), indicating that viral spread at the injection site was largely contained within the boundaries of the VTA.

We observed few Chat-positive neurons projecting to the VTA (Fig. 1d and Extended Data Fig. 2) from the PPTg and LDTg, two brain regions shown to provide robust cholinergic modulation of the VTA[28]. It is possible that the CAV2 viral-based approach has differential tropism for these neurons. To address this question, we crossed the Chat-Cre mouse with the Ai14 TdTomato reporter line and injected retrogradely transported fluorescent beads (RetroBeads) into the VTA. We observed many TdTomato-positive neurons in the PPTg and LDTg and labeled numerous cells with RetroBeads in these regions, but very few Chat neurons expressing tdTomato co-labelled with RetroBeads (Extended Data Fig. 2). Thus, although acetylcholine has a major influence on dopamine neuron activity, it appears to be derived from a relatively small number of neurons.

To further validate our retrograde CAV2 labeling we injected RetroBeads into the VTA and performed RNAscope fluorescence *in situ* hybridization to label Vgat- and Vglut2-positive neurons in select regions that we observed have either biased GABAergic input over glutamatergic input (the BNST and LPO), or equivalent GABAergic and glutamatergic input (the PAG). Consistent with our CAV2 labeling, retrogradely labeled GABAergic neurons significantly outnumbered glutamatergic neurons in the BNST and LPO, and we found approximately equal numbers of retrogradely labeled GABAergic and glutamatergic neurons in the PAG (Extended Data Fig. 3).

We found relatively few Vglut3-positive neurons projecting to the VTA from the DRN. Previous studies have shown a large number of Vglut3-positive neurons projecting from the DRN to the VTA[29] and a high degree of overlap between Vglut3 and the serotonergic marker TPH[29,30]. We found a significantly higher number of ePet1-positive serotonin neurons than Vglut3-positive neurons (Extended Data Fig. 3), which is inconsistent with these previous reports. To investigate this further, we injected mice with RetroBeads and performed RNAscope *in situ* hybridization for Vgat and Vglut3, or Vgat and Vglut2. Consistent with our CAV2 mapping we observed more retrogradely labeled Vgat-positive neurons than Vglut2-positive neurons in the DRN (Extended Data Fig. 3); however, we observed significantly more Vglut3-positive neurons than Vgat-positive neurons, consistent with previous observations[29]. These findings indicate a more reliable identification of Vgat- and Vglut2-positive neurons using Vgat- and Vglut2-Cre relative to the Vglut3-Cre line. Both Vgat- and Vglut2-Cre drivers are IRES-Cre knock-in lines as opposed to Vglut3-Cre, which is a BAC transgenic. Whether this is the reason for the reduced efficiency, or whether it is the result of tropism is unclear. Because of the efficacy of ePet1-Cre in identifying inputs to the VTA from the DRN and the high degree of Vglut3 co-expression in serotonin neurons it seems unlikely that tropism is the predominant, or only, cause of the observed discrepancy.

## Differential glutamatergic and GABAergic innervation of the VTA

To confirm our retrograde analysis in Vgat-Cre, Vglut1-Cre, and Vglut2-Cre mice, we injected approximately half of the regions where projection neurons were identified (12 GABAergic and 6 glutamatergic) with the synaptic tracer AAV1-FLEX-Synaptophysin-GFP (Syn-GFP; Fig. 2 and Supplementary Fig. 1–3). Consistent with our retrograde tracing, we observed the greatest density of Syn-GFP puncta in the VTA from GABAergic inputs (Extended Data Fig. 4). Analysis of CAV2-FLEX-ZsGreen cell number in a given region versus Syn-GFP integrated pixel density of VTA projections from that region revealed a strong correlation (Pearson $r = 0.7$, $P < 0.01$), with the exception of inputs from Vglut1::PFC (Extended Data Fig. 4). For the DStr we observed no measurable Syn-GFP projections in the VTA (Extended Data Fig. 4); therefore, this structure was excluded from correlational analysis. For the PFC we did observe Syn-GFP puncta (Fig. 2), but to a lesser extent than predicted based on the large number of retrogradely labeled cells. Vgat::DStr and Vglut1::PFC send strong inputs to regions directly adjacent to the VTA: the substantia nigra pars reticulata (SNR) and the pontine nucleus, respectively (Extended Data Fig. 4). This result highlights a caveat to this strategy where a small amount viral spread outside the boundaries of the target region can lead to false positive labeling. However, our projection

analysis with AAV1-FLEX-Synaptophysin-GFP confirmed direct projections in 17 of 18 retrogradely labelled sites, validating the overall utility of this technique.

Analysis of Syn-GFP labelled inputs revealed heterogeneity along the rostral-caudal axis of the VTA and within previously defined subdivisions (Supplementary Fig. 4 and 5) particularly from GABAergic inputs. To better resolve this heterogeneity, we compared the mean pixel intensities (normalized to peak) associated with three major subdivisions of the VTA (Fig. 2a): the VTAR, PN, and PBP. Only 1 of 6 Vglut projections tested showed significant differential innervation of different subregions (PFC, Fig. 2b). By contrast, 9 of 11 Vgat-positive projections showed statistically significant differential innervation (Fig. 2c).

## Differential synaptic connectivity of glutamatergic and GABAergic inputs

To determine the synaptic connectivity patterns of inputs to the VTA, we targeted expression of channelrhodopsin (ChR2) to 11 regions that displayed the highest level of input or most regionally restricted innervation (4 glutamatergic and 7 GABAergic). To target glutamatergic neurons, Vglut1 or Vglut2 Cre mice were crossed with mice expressing Flp recombinase under the control of the tyrosine hydroxylase (*Th*) promoter (a dopamine neuron marker)[31]. AAV1-FLEX-ChR2-YFP was injected into the region of interest, and the Flp-dependent virus AAV1-FLEXfrt-mCherry was injected into the VTA to label dopamine neurons (Fig. 3a–b). Analysis of light-evoked excitatory post-synaptic currents (Li-EPSCs) revealed that Vglut2 inputs to the VTA from the LDTg and PPTg showed a significant connectivity bias to dopamine neurons over non-dopamine neurons, with PPTg inputs being the strongest (Fig. 3c–d and Extended Data Fig. 5). By contrast, Vglut2 inputs from the rostral LH to the VTA exhibited a significant connectivity bias to non-dopamine neurons, similar to previous reports[20]. Surprisingly, Li-EPSCs from mPFC inputs were nearly undetectable (< 5 pA) in most dopamine and non-dopamine neurons (Fig. 3d).

To determine the efficacy of specific inputs in regulating dopamine neuron firing, action potentials were recorded in response to 20-Hz light stimulation. Although we observed a projection bias of glutamatergic inputs from the PPTg and rostral LH, stimulation of these terminals significantly increased action potential firing in both dopamine and non-dopamine neurons (Fig. 3e–g). Stimulation of LDTg inputs, which were weaker than those from the PPTg, did not significantly increase firing in non-dopamine neurons and was not reliable at evoking increased action potential firing in dopamine neurons (Fig. 3h).

To our surprise, mPFC inputs that did not reliably evoke detectable Li-EPSCs drove significant increases in action potential firing in both dopamine and non-dopamine populations (Fig. 3i). Consistent with this observation, we detected reliably evoked Li-EPSCs in dopamine and non-dopamine neurons following the 20 Hz stimulus trains (Fig. 3j). Recording Li-EPSCs during the stimulus train showed a strongly facilitating synapse (paired pulse ratio >1), in contrast to inputs from the PPTg, which were depressing (Fig. 3k and l). Stimulus trains of 10 Hz, but not 5 Hz, were sufficient to induce this significant increase in amplitude (Extended Data Fig. 5). We found that the amplitude of enhanced PFC Li-EPSCs was maintained for at least 30 minutes following stimulation; by contrast, repetitive stimulation of PPTg inputs did not cause a significant increase in response

amplitude (Extended Data Fig. 5). The enhancement and maintenance of Li-EPSC amplitude was not blocked in the presence of the NMDA receptor antagonist AP5 (Extended Data Fig. 5), suggesting it is not an NMDA receptor-dependent mechanism.

To establish the synaptic connectivity of GABA inputs to the VTA, Vgat-Cre mice were injected with AAV1-FLEX-ChR2-mCherry into the region of interest and AAV1-FLEX-YFP into the VTA to label GABA neurons for patching. Analysis of light-evoked inhibitory post-synaptic currents (Li-IPSCs) revealed robust connectivity from local VTA GABA neurons to non-GABA VTA neurons (Fig. 4a). In contrast, all GABAergic inputs from outside the VTA showed a preferential connectivity bias towards VTA GABA neurons compared to non-GABA neurons, with the exception of the VP, which showed no significant bias (Fig. 4a and Extended Data Fig. 5) consistent with previous observations[22].

We next recorded changes in action potential firing during 20 Hz stimulation (Fig. 4b). Due to the relative homogeneity of synaptic connectivity of distal GABAergic inputs, we pooled these samples for simplicity. Consistent with the connectivity bias of these inputs, we observed significant suppression of action potential firing in VTA GABA neurons, but much weaker suppression in non-GABA neurons (Fig. 4c). In contrast, local GABA neurons potently suppressed the action potential firing of non-GABA neurons (Fig. 4d).

These results suggest that local GABA-producing neurons within the VTA/RMTg predominantly synapse onto non-GABA-producing neurons while descending GABAergic inputs predominantly synapse onto local GABAergic neurons within the VTA. We were unable to assess the degree to which local GABAergic neurons synapse onto other GABA-releasing neurons within the region because of ChR2 expression within neighboring cells. To better resolve this we devised a genetic strategy to selectively inactivate GABA release from local or distal GABA sources (Fig. 4e). To achieve this, we crossed a mouse line in which the gene encoding Vgat (*Slc32a1*) is flanked by loxP sites with the $Th^{FlpO}$ mouse line to generate $Vgat^{lox/lox}$::$Th^{FlpO/+}$ mice. Control mice were injected in the VTA with a non-functional Cre virus (AAV1-ΔCre-GFP) along with AAV1-FLEXfrt-mCherry to label dopamine neurons. To inactivate local sources of GABA release, we injected AAV1-Cre-GFP and AAV1-FLEXfrt-mCherry into $Vgat^{lox/lox}$::$Th^{FlpO/+}$ mice. To inactivate distal GABA release, we injected CAV2-Cre along with AAV1-FLEXfrt-mCherry and AAV1-FLEX-Vgat into $Vgat^{lox/lox}$::$Th^{FlpO/+}$ mice. Because CAV2 does infect neurons at the site of injection (Extended Data Fig. 1), we included a “rescue” virus (AAV1-FLEX-Vgat) to restore Vgat expression to neurons within the VTA that were infected with CAV2-Cre[32].

To validate the effectiveness of these viral strategies we utilized RNAscope *in situ* hybridization to label Cre-positive and Vgat-positive neurons in the VTA. AAV1-Cre-GFP reduced the number of Vgat-expressing neurons in the VTA to 18.4% of control, with 2.1% of Cre-positive cells expressing Vgat. By contrast, injection of CAV2-Cre+AAV1-FLEX-Vgat restored the number of Vgat-positive neurons above control levels, with 99.4% of Cre-positive cells expressing Vgat (Extended Data Fig. 6).

To establish the impact of inactivating GABA release from local versus distal sources, we patched Th-positive and Th-negative neurons within the VTA and recorded mIPSCs.

Inactivation of Vgat within the VTA reduced mIPSCs on Th-postive neurons by approximately 60% (Fig. 4f) but had no significant effect on mIPSCs recorded from Th-negative neurons (Fig. 4g), suggesting little connectivity between local GABAergic neurons and non-dopamine producing neurons within the region. Inactivation of Vgat from distal sources significantly reduced synaptic GABA release onto Th-positive neurons (Fig. 4f), suggesting that the small Li-IPSCs recorded from all descending inputs to non-GABA neurons (Fig. 4a) sum to approximately 40% of all synaptic inhibitory contact onto dopamine-producing cells. Consistent with the strong bias of Li-IPSCs onto GABAergic neurons of the VTA, inactivation of distal GABA release reduced mIPSCs by over 80% onto Th-negative neurons (Fig. 4g). Neither manipulation affected mIPSC amplitude (Fig. 4f–g). These data indicate that dopamine neurons receive significant GABAergic input from both local and distal sources, while GABAergic input onto VTA GABA neurons arises almost entirely from distal sources.

## Distal and local GABA inputs to the VTA differentially regulate behavior

Our ability to genetically inactivate GABA release from local or distal sources allowed us the unique opportunity to investigate how these sources impact behavior. We previously demonstrated that disruption of local GABAergic networks within the VTA profoundly alters psychomotor behavior[18]. Consistent with this observation, inactivation of local GABA release resulted in high levels of basal locomotor activity, while inactivation of release from distal GABA sources had little effect on this behavior (Extended Data Fig. 6).

GABA in the VTA is increasingly linked to the regulation of psychomotor responding to cocaine[4,18,33,34]. To determine whether local or distal GABA differentially impact psychomotor sensitization to cocaine, mice were injected (20 mg/kg, subcutaneous) once daily for five-consecutive days (Fig. 5a). Cocaine elicited a robust paradoxical calming of hyperlocomotor activity in local GABA KO mice (Fig. 5b–c). In contrast, cocaine injection resulted in increased locomotor responding in control and distal GABA KO mice that increased across days (Fig. 5b–c). This effect was potentiated in distal GABA KO mice (Fig. 5b–c).

To determine whether local or distal sources of GABA to the VTA differentially impact basic reward-related behavior, we tested mice in a simple Pavlovian conditioning paradigm in which presentation of an auditory and visual cue (lever extension) co-terminated with delivery of a sucrose pellet reward (Fig. 5d). Control mice demonstrate a learned association between the cue and reward by making increased anticipatory head entries into the food hopper during the cue presentation (Fig. 5e). In contrast, local GABA KO mice failed to demonstrate a conditioned reward association (Fig. 5f). Distal GABA KO mice learned this association at a similar rate to controls (Fig. 5g). Although local GABA KO mice are hyperactive, their total head entries during each session did not differ from controls or distal GABA KO mice (Extended Data Fig. 6).

Following Pavlovian conditioning mice were switched to an operant paradigm in which reward delivery (one sucrose pellet) was contingent on making a single lever press (FR1) on either of the extended levers (Fig. 5h). Over three days of training there was no difference in

total lever pressing between control and the distal GABA KO mice (Extended Data Fig. 6), but local GABA KO mice pressed at a significantly higher rate (Extended Data Fig. 6).

Next, we asked whether mice could distinguish between a high or low value reward. If given a choice between two levers in an operant task, most mice will display a strong and consistent preference (~75%) for one lever or the other. We observed a strong lever bias in all three groups of mice (Extended Data Fig. 6). After the three days of operant conditioning mice were subjected to a lever switching task in which a press on their preferred lever continued to deliver a single pellet, while a press on their non-preferred lever delivered three pellets. Following 5 days of conditioning, control mice switched their preference to the high reward lever (Fig. 5i). Local GABA KO mice maintained a persistent preference for the originally preferred (low-reward) lever (Fig. 5j). Likewise, distal GABA KO mice did not switch their preference, though they were not as perseverant as local GABA KO mice (Fig. 5k).

In addition to Pavlovian reward association, the VTA is also implicated in discriminatory fear learning[35]. To assess whether Pavlovian threat discrimination is impacted by local or distal GABA knockout, mice were assessed in a discriminatory threat conditioning paradigm[35] in which a conditioned stimulus (CS)+ tone was paired ten times with unconditioned stimulus (US; 0.3 mA footshock) delivery. Ten CS− tone presentations were randomly interleaved with CS+/US pairings. Following two days of conditioning, both control and distal GABA KO mice could discriminate between the CS+ and CS−, as measured by time spent freezing during cue presentation. Local GABA KO mice did not discriminate between CS+ and CS−, displaying similar freezing response to both cues (Extended Data Fig.6).

In addition to the regulation of reward learning, dopamine plays an important role in regulating social behaviors[36] and descending disinhibitory inputs from the MPO have been shown to play an important role in this process[21]. To determine whether local or distal GABA KO differentially impact social behavior, we tested mice in a three-chamber task to measure social preference and social recognition. Following a period of habituation to a three chambered arena, an unfamiliar mouse contained within a small wire cage was placed in one chamber and an empty cage (object) was placed in the opposite chamber (Fig. 5l). Exploratory behavior was measured for 5 min. Local GABA KO mice showed the highest level of preference for the novel mouse over the novel object (Fig. 5m–n). Distal GABA KO mice showed no preference (Fig. 5m–n). Next, mice were allowed to habituate to the unfamiliar mouse for a period of 30 min., after which a novel mouse was placed in the chamber in the empty cage (Fig. 5l). Control mice and local GABA KO mice showed a significant preference for the novel mouse over the familiar mouse, while distal KO mice did not show a preference for either mouse (Fig. 5o–p).

## Individual GABAergic inputs differentially regulate dopamine-dependent behaviors

Our projection mapping analysis revealed that distal GABA inputs display differential innervation of VTA subdivisions. To determine whether a subset of these inputs differentially influence reinforcement behavior, we conditionally expressed ChR2 in four brain regions with different innervation patterns: the LS, which predominantly innervates the

VTAR, the NAc M. Shell (mSh) and MPO, which predominantly innervate the PN but have subtly different innervation of the PBP, and the LH, which had the most broadly distributed innervation pattern (Figure 2).

Vgat-Cre mice were injected with AAV1-FLEX-YFP (control) or AAV1-FLEX-ChR2-YFP in the indicated regions and fiber optic cannulas were implanted above the VTA (Figure 6a and Supplementary Fig. 6–7). Blue light stimulation (20 Hz, 5 ms pulses for 20 minutes) led to an increase in cFos-positive dopamine neurons in VTA subregions with strong ChR2-fiber innervation (Figure 6b and Extended Data Fig. 7). Only mice injected with ChR2 in the LH showed a significant increase in cFos in the PBP, while mice injected in the LH, the NAc mSh, and the MPO all showed an increase in cFos in the PN. We did not observe a significant increase in cFos staining in mice injected in the LS. Intriguingly, in LH, NAc, and MPO-injected mice the region with the highest number of cFos-positive neurons was the small interfasicular nucleus (IF), located between the two halves of the paranigral subdivision (Figure 6b and Extended Data Fig. 7).

To directly compare behavioral outcomes associated with activation of these inputs, we first tested mice in a real-time place preference (RTPP) assay. Blue light stimulation (20 Hz) of LH or MPO GABA inputs, but not LS or mSh inputs, on one side of a two-chambered arena caused a robust place preference (Figure 6c–d). VTA stimulation of mSh inputs caused a significant increase in shuttles between chambers (Figure 6e) that was associated with an increase in distance traveled (Figure 6f). MPO mice did not show a significant increase in shuttles (Figure 6e) but did show increased locomotor activity (Figure 6f). In contrast, LH mice showed a significant decrease in locomotor behavior (Figure 6f). We observed that LH mice spent most of their time in the light-paired side attempting to gnaw at the walls or the doorway of the arena, similar to that described previously[20,37], which accounts for their reduced locomotion. To quantify this behavior across groups we placed each mouse in an empty cage with a single standard food pellet and delivered 20 Hz light stimulation for 20 minutes. Stimulation of LH inputs resulted in a robust gnawing of the food pellet and accumulation of pellet dust on the cage floor, as evidenced by the significant reduction in the weight of the pellet (Figure 6g). This effect was not observed with stimulation of other inputs to the VTA.

To further probe the extent to which activation of these inputs is reinforcing, mice were assayed in a simple fixed ratio schedule of optical self-stimulation. Mice were given one hour of training per day for five days in which a single lever press on either extended lever resulted in 3 seconds of 20 Hz light stimulation. LH mice exhibited robust lever pressing behavior, while MPO and NAc mice exhibited moderate lever pressing that eventually reached statistical significance relative to YFP control mice (Figure 6h–i). For the three groups of mice that showed significant self-stimulation, we next switched their preferred lever from 20 Hz stimulation to 7 Hz stimulation, similar to the 3 pellet vs 1 pellet lever switching task described above. All three groups of mice rapidly switched to their non-preferred lever in order to continue receiving 20 Hz stimulation, with the most rapid switching observed in LH mice (Figure 6j–l).

Inactivation of distal GABA inputs to the VTA disrupts social behavior in the three-chamber assay. To assess which if any of the 4 inputs to the VTA influence this behavior we assessed mice with optical inhibition of the inputs using the inhibitory opsin Jaws[38]. Vgat-Cre mice were injected with AAV1-FLEX-Jaws-GFP or AAV1-FLEX-YFP (control) into the same four input regions and fiber optics were implanted over the VTA (Figure 6m and Supplementary Fig. 6–7). Red light activation of Jaws (2 sec on, 1 sec ramp down, 2 sec off[35]) in one chamber of a two-chamber arena did not cause a significant preference or aversion in any group (Extended Data Fig. 7). During the 3-chamber social preference assay mice received red light whenever they were in the chamber containing the target mouse (Figure 6n). Inhibition of mSh and MPO inputs disrupted social preference that was not observed in the other groups (Figure 6o). Next, we probed whether inhibition during social preference would disrupt social recognition, when inputs were no longer actively inhibited. Inhibition of MPO and mSh inputs during social preference testing impaired social recognition that was not observed in the other groups (Figure 6p).

## Discussion

The VTA receives synaptic input from a large number of brain regions that converge on this critical structure and enable the complex encoding of information in the form of precise patterns of dopamine neuron firing and downstream dopamine release[2,5,8,10,12,13,39,40]. Though previous studies have identified inputs to specific cell types and/or subregions of the VTA[8,10,12,13], here we provide a large-scale map of the neurotransmitter identity of these VTA afferents. From these findings we have gained a new understanding of how inputs to the VTA are organized, with the strongest glutamatergic inputs originating from descending cortical projections and ascending hindbrain projections, while inputs from most other subcortical structures are largely GABAergic. Moreover, we find that while glutamatergic inputs, with the exception of those coming from the mPFC, tend to innervate all subregions of the VTA with similar intensity, most GABAergic inputs exhibited biased innervation towards specific VTA subregions.

One potential caveat of our approach is that CAV2 may display tropism, or uneven infection of different cell types. Because we identified only a small number of VTA-projecting cholinergic cells in the LDTg and PPTg with our CAV strategy, we suspected that perhaps these neurons are not well labeled by this virus. However, we identified a similarly small number of Chat-positive cells labeled by RetroBeads, indicating that this result is likely accurate, and that a small number of cholinergic neurons in this region are responsible for the VTA projection. This does not discount the importance of cholinergic regulation of the VTA. Indeed, cholinergic inputs to the VTA regulate reward reinforcement[28], and potently influence dopamine neuron activity patterns[41]. It is also possible that CAV displays varying tropism for either GABA or glutamatergic neurons. However, combining RetroBead labeling with *in situ* hybridization for Vgat and Vglut2 in select regions confirmed the overall pattern of results we saw with CAV labeling. Our results are largely consistent with a previous analysis of glutamatergic inputs to the VTA in rats using wheat germ agglutinin (WGA) retrograde tracing[15]. Although these investigators found different contributions of glutamatergic inputs to the VTA, such as a greater overall proportion of glutamatergic projections from the LH relative to hindbrain inputs, they also observed a majority of

retrogradely labeled neurons in subcortical regions were not glutamatergic. The exact reason for these observed differences is not clear but may reflect differences in the species investigated (rat versus mouse), the injection site location, or the retrograde tracing method.

We observed that many of the GABAergic inputs to the VTA synapse strongly onto GABA neurons and more weakly onto non-GABA neurons. Previous studies examining individual regions including the NAc, BNST, and LH have seen similar results[11,19–23]. The VTA also contains a significant population of glutamatergic neurons[1], which likely make up a subset of the neurons we recorded. Future experiments utilizing combined Cre- and Flp-driver lines, such as those described here, will help to elucidate the specificity of connectivity on inputs onto these cell types.

This general organization of a weak inhibition onto dopamine neurons and a strong inhibition onto local GABA neurons could potentially generate a pattern of feed-forward disinhibition, whereby dopamine neurons are briefly hyperpolarized by direct GABA input and then are disinhibited by a reduction in local GABA tone. The initial hyperpolarization may be a critical feature whereby dopamine neurons are poised to respond to disinhibition with a stronger burst of action potentials[42]. Indeed, this model is supported by our data showing strong induction of cFos in dopamine neurons following optogenetic activation of specific GABAergic inputs.

To determine connectivity in this study we only measured fast GABA transmission through $GABA_A$ receptors. Recent studies examining NAc to VTA inputs have also identified metabotropic $GABA_B$ currents, primarily on dopamine neurons[11,33]. It is possible that other GABAergic inputs to the VTA also activate $GABA_B$ receptors, however for nearly every input previously examined, including the NAc, the net effect of stimulating the incoming GABAergic axons is disinhibition of dopamine neurons and increased dopamine release to result in reward reinforcement[15,30–34,43], indicating that the $GABA_A$ current on local GABA neurons is the predominating outcome.

Distal GABAergic inputs from a variety of subcortical regions, many of which show clear innervation bias to different VTA subregions, are well set up to encode a wide variety of precise behaviorally relevant information. Under this model, ascending cholinergic and glutamatergic projections may play a more permissive role in helping to set the rate of tonic dopamine firing and enabling bursting when coupled with disinhibition of local interneurons.

We did not observe significant effects of distal GABA inactivation on Pavlovian conditioning, though it should be noted that reducing phasic activation of dopamine neurons by ~70% through genetic inactivation of NMDA-type glutamate receptors also does not affect Pavlovian reward association[44]. This suggests potentially important redundant mechanisms whereby either glutamatergic drive onto dopamine neurons or disinhibition through distal GABAergic inputs onto local GABA neurons is sufficient to provide the minimal amount of dopamine required for this behavior.

Local, but not distal GABA knockout disrupted conditioned threat discrimination indicating that GABAergic tone onto dopamine neurons plays an important role in this process.

Consistent with this observation, glutamatergic inputs from the LH and BNST, which predominantly synapse onto VTA GABA neurons, are both aversive[19,20], and BNST glutamatergic inputs have been shown to respond to both foot shock and shock-associated cues[19]. Thus, glutamatergic inputs onto both VTA GABA neurons and dopamine neurons are likely to work coordinately in regulating threat discrimination.

We observed that inactivation of distal GABAergic inputs to the VTA disrupted discrimination between high and low rewards, suggesting that both local and distal GABAergic inputs are critical for value-based decision making. Several studies have investigated individual GABAergic inputs to the VTA[11,19–21], but whether these inputs have similar or distinct functions has not been thoroughly investigated. We observed that LH inputs, which were the most broadly distributed throughout the VTA subregions, were the most strongly reinforcing and promoted a distinct gnawing phenotype. This is consistent with previous reports of optical stimulation of LH to VTA GABA projections causing robust place preference, self-stimulation behavior, and either feeding or gnawing[20,37,45]. Our observation that LH inputs, which broadly innervate the VTA, are more reinforcing than either the MPO or NAc mSh inputs is also consistent with our recent observations that simultaneous activation of dopamine neurons in the lateral and medial parts of the VTA is required for optimal reinforcement[46].

We observed that inactivation of distal GABAergic inputs resulted in impaired social behavior that was not observed in local GABA KO mice. This suggests that distal GABA projections are important for disinhibiting local GABA to enable a dopamine signal for regulating social behaviors[47]. Indeed, we found that inhibition of specific inputs from the MPO or NAc mSh were able to disrupt social preference and social recognition, while LH and LS inputs did not affect this behavior, further supporting distinct roles for GABAergic inputs to the VTA.

The role of the rostral VTA in reward behaviors remains somewhat elusive. We did not observe any behavioral effects of activating LS inputs, which predominantly innervate the rostral VTA. We also did not observe a significant increase in cFos following activation of LS GABA inputs, though it is unclear whether this is a result of the relative strength of this input compared to others examined, or whether the connectivity of this input is distinct and less likely to lead to cFos activation via disinhibition. However, evidence suggests that LS inputs to the rostral VTA do lead to dopamine neuron disinhibition[48].

The precise behavioral role of glutamatergic inputs from the mPFC to the VTA remains unclear. We found that these inputs showed biased innervation to different VTA subregions, as well as unique synaptic properties including a persistent facilitation. These properties are strikingly different from those of PPTg inputs, which were depressed by repetitive stimulation. This variability of basic synaptic properties may facilitate different roles for different glutamatergic inputs in the control of dopamine neuron firing, particularly during learning-dependent tasks. Consistent with an important role for plasticity in mPFC inputs to the VTA for regulating associative behavior, inactivation of NMDA-type glutamate receptors in mPFC projections to the VTA potently reduces simple Pavlovian reward association[49]. Future studies designed to interrogate the interactions between mPFC inputs to the medial

VTA PN region and GABAergic disinhibitory inputs to this region will provide important new insights into the coordinate regulation of specialized dopamine projection neurons.

## Methods:

### Mice:

All procedures were approved and conducted in accordance to the guidelines of the Institutional Animal Care and Use Committee of the University of Washington. Mice were housed on a 12-hour light/dark cycle with ad libitum food and water. Approximately equal numbers of male and female mice were used for all experiments. Mice were group housed except during day/night locomotor experiments. See Supplementary Table 1 for information on mouse lines.

### Viruses:

All CAV and AAV viruses were produced in house with titers of 1–3 $\times 10^{12}$ particles per mL as described[24].

### Surgery:

Mice were anesthetized with isoflurane before and during viral injection. Mice recovered for at least 2 weeks (AAV) or three weeks (CAV) prior to experimentation. For slice electrophysiology, mice were injected at approximately 5–6 weeks of age. For all other experiments, mice were injected at 8–12 weeks of age. See Supplementary Table 2 for injection coordinates. Values are in mm, relative to bregma. Y values caudal to bregma were adjusted for bregma-lambda distance using a correction factor of 4.21 mm. For Z values the syringe was lowered 0.5 mm past the indicated depth and raised up at the start of the injection.

**Note:** We found that targeting the midpoint of the LH (−1.25 mm from Bregma) resulted in robust synaptophysinGFP labeling and synaptic connectivity in Vgat-Cre mice. However, in Vglut2-Cre mice we only observed consistent light-evoked EPSCs in slice when targeting the most rostral aspect of the structure. This is consistent with previous reports observing functional LH-VTA glutamatergic connectivity, which also targeted the rostral LH[20].

### Retrograde Input Mapping:

At least three weeks following injection of 500 nl CAV2-FLEX-zsGreen virus into the VTA, mice were euthanized and perfused with 4% paraformaldehyde. 30 μm frozen brain sections were collected and mounted on glass slides. One brain section per atlas page[25] was imaged at 10x magnification using a Keyence BZ-X710 fluorescent microscope and cells in each brain region were counted by an experienced investigator. Brain regions were included if we observed retrograde labeling in at least half of injected animals.

### Synaptophysin-GFP Input Mapping:

At least two weeks following injection of AAV1-FLEX-synaptophysinGFP (300 nl), mice were euthanized and perfused with 4% paraformaldehyde. 30 μm frozen brain sections were collected. One section per atlas image for the rostral-caudal extent of the VTA was selected

and stained overnight with a Rabbit anti GFP antibody (Invitrogen A11122, 1:2000). Images were collected at 10x magnification using a Keyence BZ-X710 fluorescent microscope and analyzed using ImageJ software. Images were background subtracted and mean pixel intensity and integrated pixel density were measured for each VTA subregion. For normalized intensity plots all subregions from an individual animal were normalized to the highest intensity subregion from that animal.

### RNAscope *in situ*:

For *in situ* combined with RetroBeads, mice were stereotaxically injected in the VTA with red RetroBeads (Lumafluor). Two weeks following injection brains were collected and snap frozen, and 20 μm sections were mounted onto slides. The RNAscope version 1 assay (Advanced Cell Diagnostics) was performed according to manufacturer's directions using probes directed against *Slc32a1* (Vgat), *Slc17a6* (Vglut2), or *Slc17a8* (Vglut3). For *in situ* to asses gene knockout, $Vgat^{lox/lox}$ mice were injected in the VTA with AAV1-ΔCre-GFP, AAV1-Cre-GFP, or CAV-Cre+AAV1-FLEX-Vgat. Three weeks following injection brains were collected and snap frozen, and 20 μm sections were mounted onto slides. The RNAscope version 2 assay (Advanced Cell Diagnostics) was performed according to manufacturer's directions using probes directed against *Cre* and *Slc32a1* (Vgat).

### Slice Electrophysiology:

Horizontal or coronal brain slices (200 or 250 μm, respectively) were prepared in an ice slush solution containing (in mM): 92 NMDG, 2.5 KCl, 1.25 $NaH_2PO_4$, 30 $NaHCO_3$, 20 HEPES, 25 glucose, 2 thiouria, 5 Na-ascorbate, 3 Na-pyruvate, 0.5 $CaCl_2$, 10 $MgSO_4$, pH 7.3–7.4[50]. Slices recovered for ≤12 minutes in the same solution at 32°C and then were transferred to a room temperature solution including (in mM): 92 NaCl, 2.5 KCl, 1.25 $NaH_2PO_4$, 30 $NaHCO_3$, 20 HEPES, 25 glucose, 2 thiouria, 5 Na-ascorbate, 3 Na-pyruvate, 2 $CaCl_2$, 2 $MgSO_4$. Slices recovered for an additional 45 minutes before recordings were made in ACSF at 32°C continually perfused over slices at a rate of ~2 ml/min and containing (in mM): 126 NaCl, 2.5 KCl, 1.2 $NaH2PO_4$, 1.2 $MgCl_2$ 11 D-glucose, 18 $NaHCO_3$, 2.4 $CaCl_2$. All solutions were continually bubbled with $O_2/CO_2$.

Whole-cell recordings were made using an Axopatch 700B amplifier (Molecular Devices) with filtering at 1 KHz using 4–6 MΩ electrodes. For mIPSC recordings electrodes were filled with an internal solution containing (in mM): 135 KCl, 12 NaCl, 0.5 EGTA, 10 HEPES, 2.5 Mg-ATP, 0.25 Na-GTP, pH 7.3, 280 mOsm. For light-evoked EPSC, IPSC, and action potential recordings electrodes were filled with an internal solution containing (in mM): 130 K-gluconate, 10 HEPES, 5 NaCl, 1 EGTA, 5 Mg-ATP, 0.5 Na-GTP, pH 7.3, 280 mOsm.

mIPSC recordings were made with holding at −60 mV in the presence of tetrodotoxin (500 nM) and kynurenic acid (2 mM). Events were analyzed using MiniAnalysis software (Synaptosoft) using automated detection with visual confirmation by an experienced investigator.

Light-evoked synaptic transmission was induced with 5 ms light pulses delivered at 0.1 Hz from an optic fiber placed directly in the bath. Light-evoked EPSCs were measured with

holding at −60 mV in the presence of picrotoxin (100 μM). Light-evoked IPSCs were measured with holding at −30 mV. Amplitudes were calculated from an average of at least 10 events. Spontaneous action potentials were recorded in current clamp mode in the same neurons used for EPSC/IPSC recordings. 20 Hz trains of 5 ms light pulses were delivered for 1 second (20 pulses) once every 10 seconds to determine the effect of light on action potential firing rates. Pre- and post-train firing rates were calculated for the two seconds immediately preceding and following the light train, respectively, and were an average of at least three sweeps.

mIPSC recordings and light-evoked EPSC recordings for Vglut1 and Vglut2 were performed in mice expressing FlpO recombinase under the control of the tyrosine hydroxylase (TH) promoter. Dopamine and non-dopamine neurons were identified by the presence or absence (respectively) of a Flp-dependent fluorescent marker delivered by AAV (AAV1-FLEXfrt-mCherry). Light-evoked IPSC recordings were performed in Vgat Cre mice, and GABA- and non-GABA neurons were identified by expression of a Cre-dependent fluorescent marker delivered by AAV (AAV1-FLEX-GFP).

### Behavioral Assays in Vgat$^{lox/lox}$ mice:

**Locomotion:** Mice were singly housed in standard cages with food and water provided that were placed inside infrared locomotion chambers (Columbus Instruments). Ambulatory activity (beam breaks) was measured in 15-minute bins continuously for three nights and two days.

**Cocaine Sensitization:** Mice were placed into a standard cage inside infrared locomotion chambers (Columbus Instruments). The cage was clean on the first day, and the same cage was used for all subsequent days. After 90 minutes mice were injected subcutaneously with saline or 20 mg/kg cocaine. Mice received two days of saline injections followed by five days of cocaine injections. The second saline day is plotted in the figure. Ambulatory activity (beam breaks) was measured in 5-minute bins.

**Pavlovian Conditioning:** Mice were food restricted to 85% of their ad libitum body weight. Mice were placed into operant conditioning boxes (Med Associates) and received 25 trials/day for 7 days. Each trial consisted of both levers extending (an auditory and visual cue) and remaining extended for 10 seconds, at which point both levers retracted and a single 20 mg reward pellet was delivered (unflavored Purified Dustless Precision Pellets, Bio-Serv). Trials were separated by a variable inter-trial interval averaging 60 seconds. Head entries during the cue period and the inter-trial interval were measured using an infrared detector in the food hopper.

**Instrumental Responding:** Following Pavlovian training, mice were placed in the same operant boxes. Both levers extended and remained extended until a press was made on either lever, at which point both levers would retract and one pellet was delivered. Levers would re-extend when the mouse made a head entry into the food hopper. Mice were given a 1-hour session each day for three days.

**Lever Switching:** Each mouse's non-preferred lever was determined based on their performance on day 3 of instrumental training. The non-preferred lever was set as the high reward lever (3 pellets) and the preferred lever was set as the low reward lever (1 pellet). Mice were given 25 trials in which both levers extended; following a press on either lever both levers would retract and the appropriate reward was delivered, followed by a one minute inter-trial interval before the levers extended for the next trial.

**Fear Conditioning:** Fear conditioning was performed as described[35]. Briefly, mice were placed into Context A and baseline freezing was measured across 3 presentations of the CS+ tone and 3 presentations of the CS− tone. Tones were counterbalanced across groups. Mice then received two days of conditioning in Context B, consisting of 10 presentations of the CS+ tone (10 s) coterminating with a 0.5 s footshock (0.3 mA) and 10 presentations of the CS− tone. The day following the second conditioning session mice were returned to Context A and freezing was measured during 3 presentations of each CS. Movement was tracked using Ethovision software (Noldus) and freezing calculated using a custom Matlab script.

**3 Chamber Social Assay:** The arena was a white Plexiglas box (60 cm × 30 cm × 30 cm) divided into three equal sized chambers with clear Plexiglas dividers, each with a doorway allowing the mice to freely pass between chambers. Mice were given 10 min to explore the empty arena, then were briefly removed and returned to their home cage while the novel object (empty wire pencil cup) was introduced to one chamber and first mouse (contained in a wire pencil cup) was introduced to the opposite chamber. The experimental animal was returned to the arena for a 30-minute exploration, of which the first five minutes were scored, and then briefly removed again while the novel mouse was added, before a final five-minute exploration.

### Optogenetic Behavioral Experiments:

Vgat-Cre mice were injected bilaterally in the indicated region with 400 nl AAV1-FLEX-ChR2-YFP or AAV1-FLEX-Jaws-GFP. Control mice were injected with AAV1-FLEX-YFP. Optic fibers were implanted bilaterally above the VTA, with one fiber implanted at a 10° angle to allow enough working room between ferrules to attach patch cables. Histology to verify targeting was performed on ChR2 and Jaws mice only.

**Real-time place preference/aversion:** On day 1 mice were placed into a two-chambered arena and allowed to explore freely for 10 minutes. The walls of the arena had horizontal black and white stripes in one chamber and vertical black and white stripes in the other chamber. Mice were then assigned a light-paired chamber such that any inherent side bias was cancelled out within groups. On day 2 mice were connected to patch cables and placed into the unpaired chamber to begin the trial. 20 Hz, 5 ms blue light stimulation (ChR2) or 2 sec on-1 sec rampdown-1 sec off red light stimulation (Jaws) was delivered whenever the centerpoint of the mouse was in the paired chamber. The trial lasted for 20 minutes.

**Intracranial Self-Stimulation:** Mice were food restricted to 85% of ad libitum body weight in order to increase exploratory activity. Mice were given a 1-hour session each day

in which both levers extended and a press on either lever led to lever retraction and 3 seconds of 20 Hz light stimulation. Levers re-extended following an additional 2 second timeout period. Following 5 days of lever acquisition the frequency of light stimulation was decreased to 7 Hz on each mouse's preferred lever, while the frequency on the non-preferred lever remained 20 Hz.

**Light-induced gnawing behavior:** Mice were placed in a clean empty cage with no bedding and given a single standard food pellet, which was weighed prior to the trial. Mice were then given 20 minutes of 20 Hz light stimulation and the food pellet was weighed again at the end of the trial.

**3 Chamber Social Assay:** Mice were connected to the patch cables and placed into the empty three-chamber arena for a 10-minute habituation period. Next the experimental mice were briefly removed from the chamber but remained connected to the patch cables while the object (empty wire pencil cup) and first mouse (under a pencil cup) were introduced to opposite chambers. Experimental mice were returned to the arena for a 30-minute period during which they received red light stimulation (2 s on, 1 s ramp down, 2 s off) whenever they were in the chamber containing the mouse. The first five minutes of this period were scored for social preference. The experimental mouse was then briefly removed from the chamber while the second mouse was added under the empty pencil cup, and the experimental mouse was returned for a final five-minute period. The mouse remained connected to the patch cables but no light stimulation was given during this period.

**cFos staining:** Mice were given 20 minutes of 20 Hz light stimulation and were perfused 1 hour following the end of the stimulation period. 30 μm sections were collected and one section per atlas image for the rostral-caudal extent of the VTA was selected and stained overnight at room temperature with antibodies against cFos (Millipore ABE457, 1:1000) and TH (Millipore MAB318, 1:1000). Images were collected at 20x magnification using a Keyence BZ-X710 fluorescent microscope and analyzed using ImageJ software.

## Statistics and Reproducibility

All data were analyzed for statistical significance using GraphPad Prism software. For multiple groups or multiple measures we used One-way or Two-way ANOVA. Tukey's multiple comparison tests were used for One-way ANOVAs with multiple comparisons across groups. Dunnett's selected comparisons were used for directly comparing experimental groups to the control group. Bonferroni's multiple comparison tests were used for between subjects comparisons following two-way ANOVA and Fisher's single comparison tests were used for a within subjects comparison. Data distribution was assumed to be normal but this was not formally tested. No statistical methods were used to pre-determine sample sizes but our sample sizes are similar to those reported in previous publications[35,46]. All behavioral assays were repeated in a minimum of three cohorts with similar replication of results. Data for imaging and electrophysiology experiments were pooled from at least three individual animals, collected from at least two rounds of experiments, with similar replication of results. Littermates were randomly assigned to experimental groups and animals were tested in a random order. Data were analyzed by an

investigator blinded to experimental condition; the experimenter was not blinded during data collection. Animals with missed viral injections or significant viral spread outside the targeted region were excluded from analyses.

## Reporting Summary

Further information on experimental design is available in the Nature Research Reporting Summary linked to this article.

## Data availability statement

Datasets supporting the findings in this study are available from the corresponding author upon reasonable request.All viral vectors used in this manuscript are available from the corresponding author upon reasonable request.

## Code availability statement

Code used for behavioral analysis is available from the corresponding author upon reasonable request.

## Extended Data

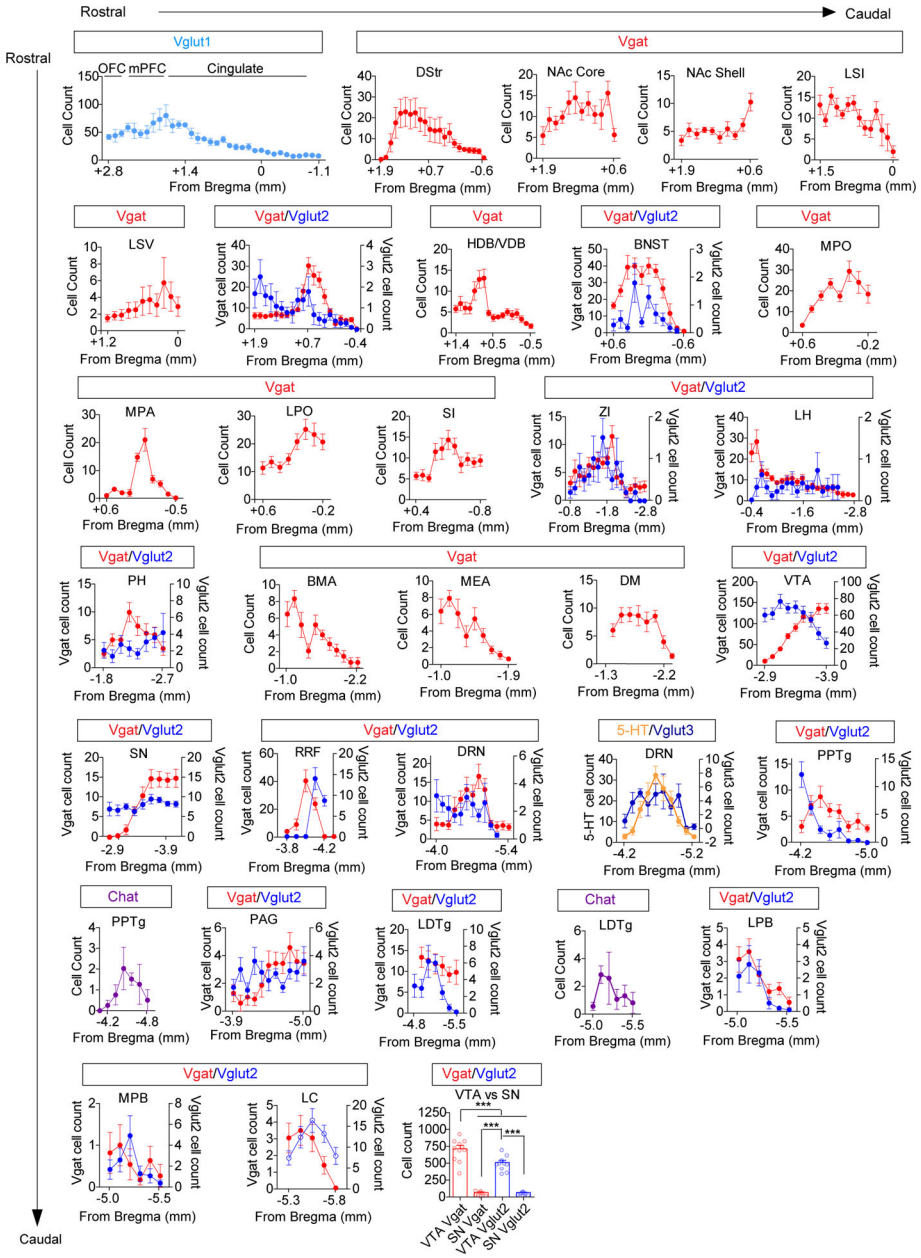


**Extended Data Fig. 1. Distribution of CAV2-FLEX-zsGreen retrogradely labeled neurons**

Cell counts of retrogradely labeled cells in indicated Cre lines across the rostral-caudal axis. Note that cells from different Cre lines in the same region are plotted on different axes. (Vgat n=11 mice, Vglut1 n=4; Vglut2 n=10; Vglut3 n=5, 5-HT n=13, Chat n=4.) Final panel depicts counts of infected cells in the VTA and neighboring substantia nigra (SN) region (Vgat n=11 mice, Vglut2 n=10 mice, One way ANOVA $F_{(3,38)}$=112.3 p<0.0001, Tukey's Multiple Comparison ***p<0.001). Error bars represent s.e.m.

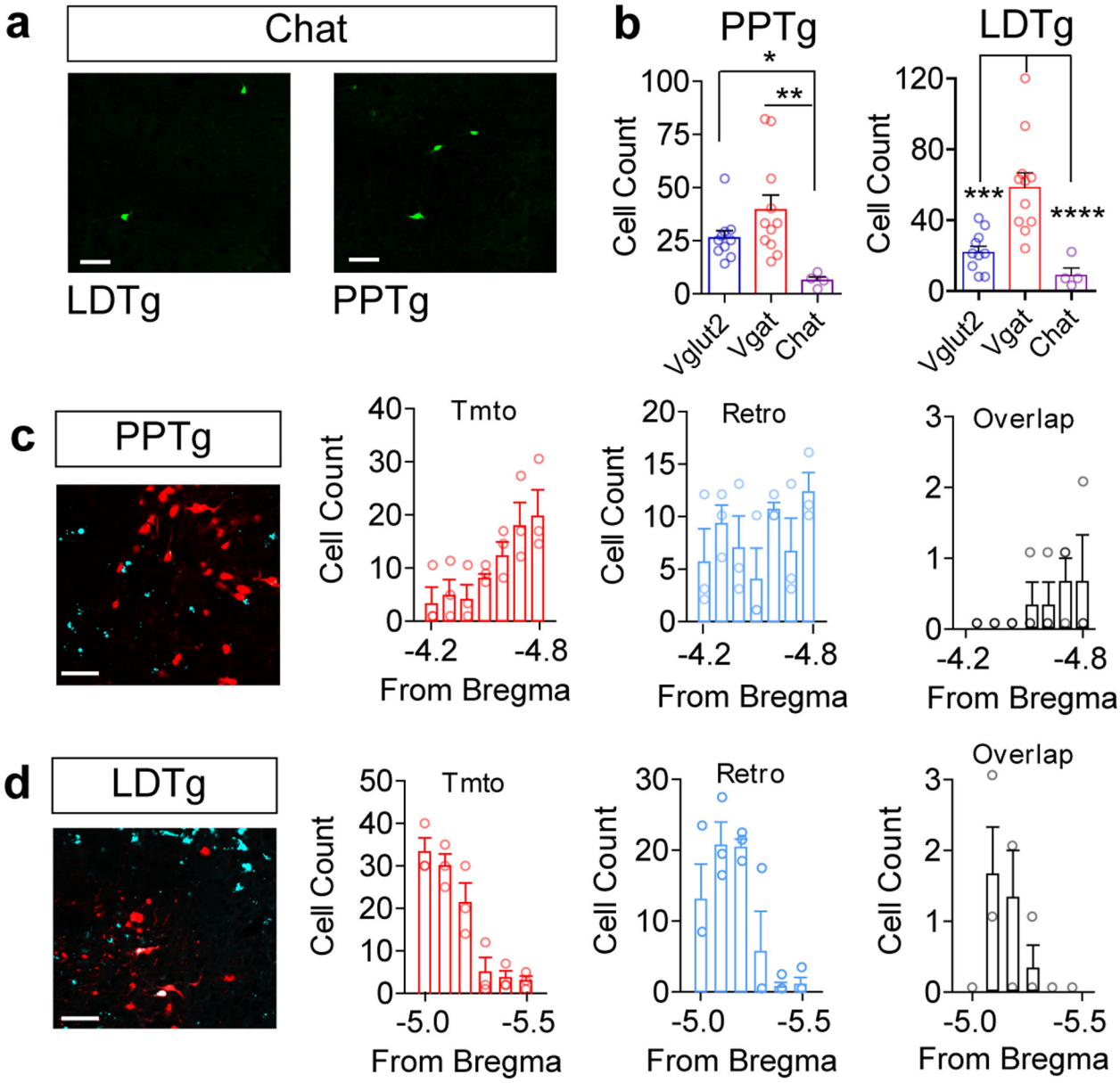


**Extended Data Fig. 2. Retrobead labeling of cholinergic neurons in the PPTg and LDTg**

**(a)** Representative image of CAV2-FLEX-zsGreen retrogradely labeled cells in the PPTg and LDTg of a Chat Cre mouse. **(b)** Total cells labeled in the PPTg and LDTg in different Cre driver lines (Vglut2 n=10, Vgat n=11, Chat n=4; PPTg, One-way ANOVA, $F_{(2,28)}$=7.740, P=0.0023, *P<0.05, **P<0.01; LDTg, One-way ANOVA, $F_{(2,28)}$=17.41, P<0.0001, ***P<0.01, ****P<0.0001). **(c-d)** Representative images of Chat Cre:Tomato cells (red) and RetroBeads from the VTA (cyan) in the PPTg and LDTg, and quantification of cell counts and overlap across the rostral-caudal axis (n=3/group). Error bars represent s.e.m. Scale bars = 50μm.

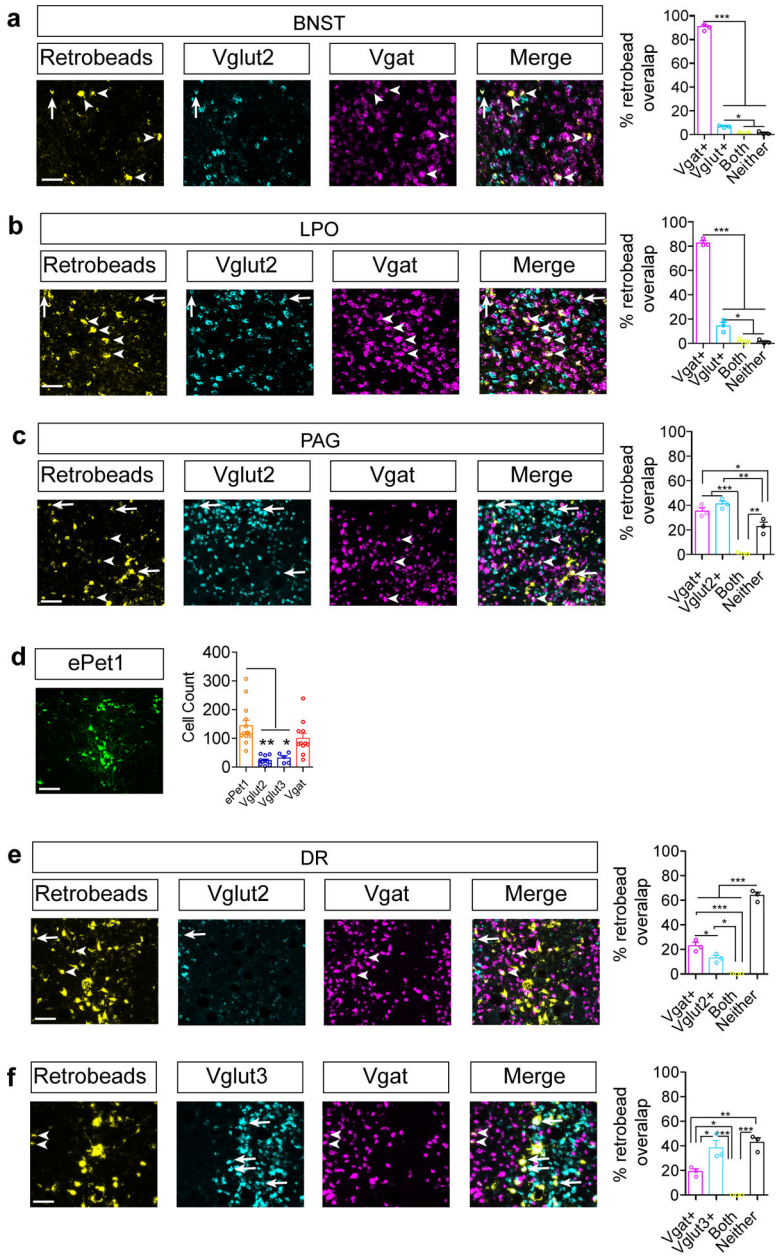


**Extended Data Fig. 3. Retrobead and *in situ* labeling of VTA inputs**

**(a-c)** Representative images of indicated regions containing RetroBeads transported from the VTA and RNAscope *in situ* against *Slc32a1* (Vgat) or *Slc17a6* (Vglut2) and quantification of the percent of RetroBead labeled cells that colabel with *in situ* probes for BNST(a), LPO(b), and PAG(c). Arrows identify RetroBead-labeled Vglut-positive neurons, while arrowheads identify RetroBead-labeled Vgat-positive neurons (n=3 mice, cells counted in 3–5 sections per region per mouse. One-way ANOVA, BNST: $F_{(3,8)}$=2140, P<0.0001, LPO: $F_{(3,8)}$=441.3, P<0.0001, PAG: $F_{(3,8)}$=48.31, P<0.0001, Tukey's Multiple Comparisons *P<0.05, **P<0.01, ***P<0.001). **(d)** Representative CAV2-FLEX-ZsGreen labeling in DR of ePet1-Cre mice (scale bar = 100 μm) and cell counts in DR for ePet1, Vglut2, Vglut3, and Vgat Cre mice (ePet n=13, Vglut2 n=10, Vglut3 n=5, Vgat n=11 mice; One-way ANOVA,

$F_{(3,35)}$=12.10, P=0.0001, Tukey's Multiple Comparisons *P<0.05, **P<0.01). **(e-f)** Representative images for DR RetroBeads transported from the VTA and RNAscope *in situ* against *Slc32a1* (Vgat), *Slc17a6* (Vglut2), or *Slc17a8* (Vglut3), and quantification of the percent of RetroBead labeled cells that colabel with *in situ* probes. Arrows identify RetroBead-labeled Vglut-positive neurons, while arrowheads identify RetroBead-labeled Vgat-positive neurons (n=3 mice, cells counted in 3–5 sections per mouse. One-way ANOVA, Vglut2: $F_{(3,8)}$=161.9, P<0.0001, Vglut3: $F_{(3,8)}$=28.94, P=0.0001, Tukey's Multiple Comparisons *P<0.05, **P<0.01, ***P<0.001). Error bars represent s.e.m. Scale bars = 50μm.

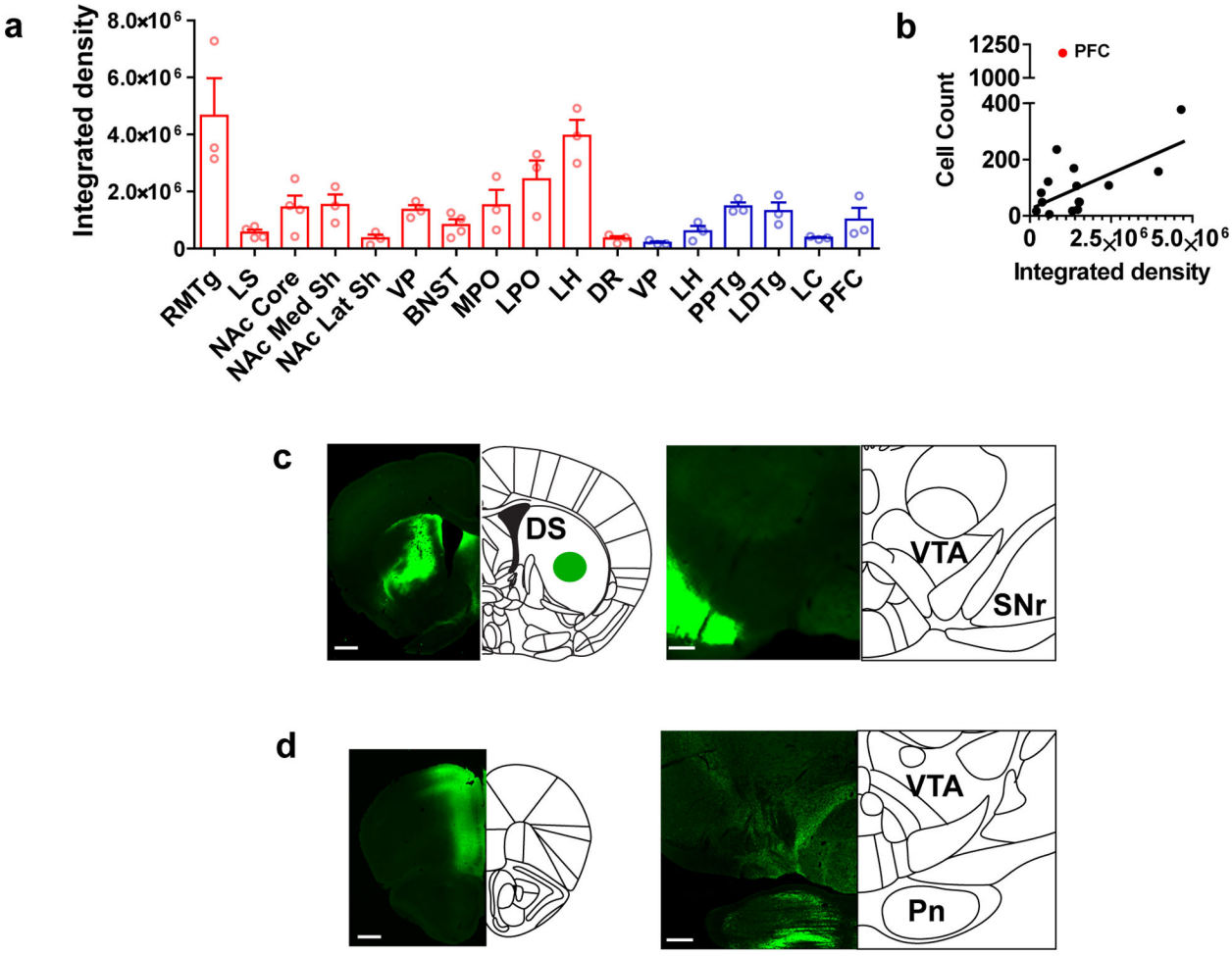


**Extended Data Fig. 4. Density of inputs to the VTA**

**(a)** Integrated density (arbitrary units) of GFP fluoresence in the VTA following injection of synaptophysinGFP into the indicated region. Red bars: Vgat Cre, blue bars: Vglut 1 or 2 Cre (n=3 mice/group for all regions except n=4 mice for LS, NAc core, and BNST). **(b)** Correlation between average total integrated fluoresence density in the VTA and the average number of cells retrogradely labeled by CAV-FLEX-ZsGreen in each region. Black line = linear regression of all points excluding PFC (n=3 mice/group for all regions except n=4 mice for LS, NAc core, and BNST; Pearson r = 0.6570, Spearman two-tailed P=0.0078). **(c)**

Representative images of synaptophysinGFP injection into the dorsal striatum of a Vgat Cre mouse, and terminals in the SNr, adjacent to the VTA. Scale bars = 500 μm (left) and 200 μm (right). **(d)** Representative images of synaptophysinGFP injection into the PFC and terminals in the VTA-paranigral region and the adjacent pontine nucleus. Error bars represent s.e.m.

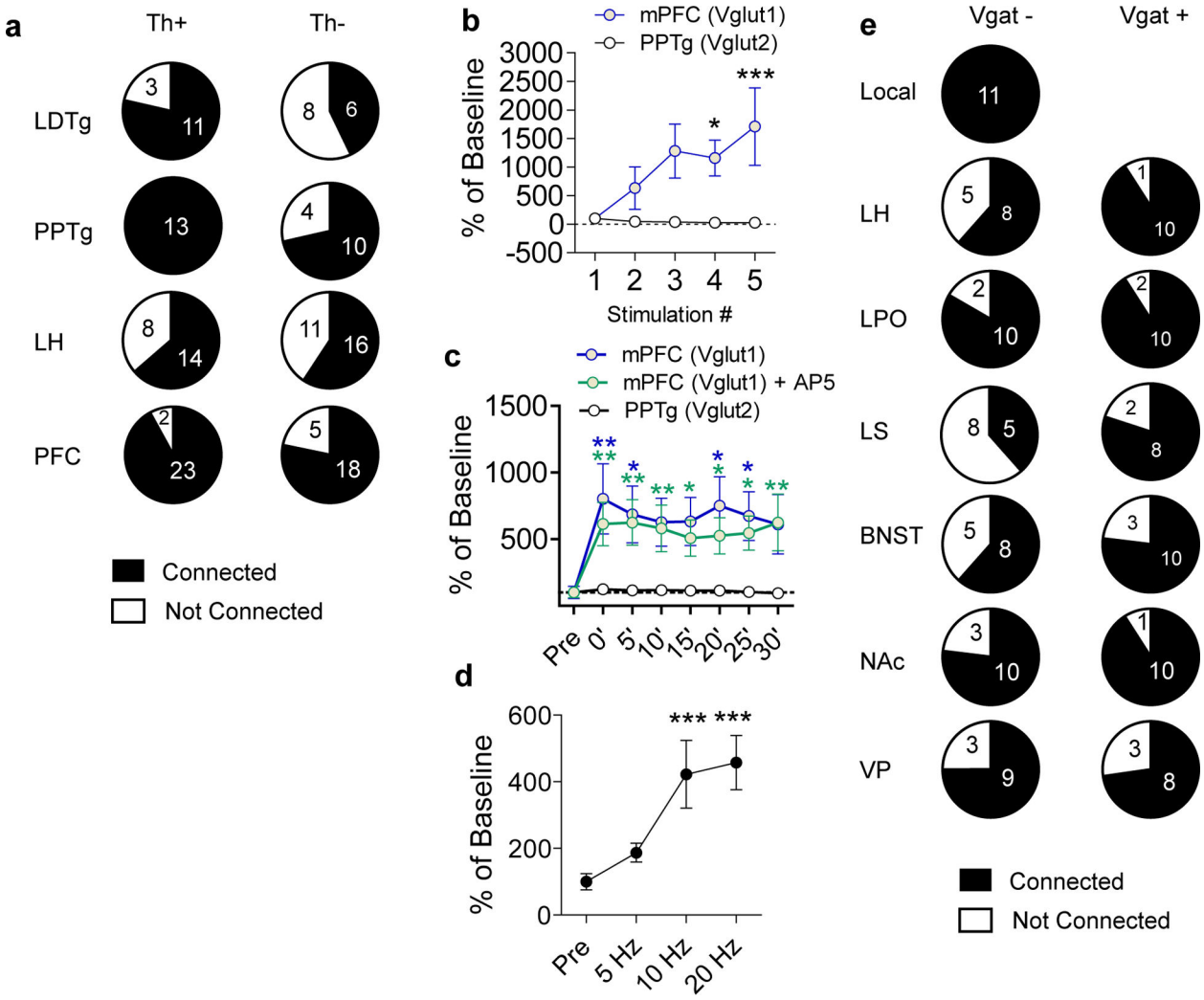


**Extended Data Fig. 5. Connectivity of VTA inputs**

**(a)** Numbers of connected and not connected Th+ and Th− cells patched in the VTA with ChR2 expressed in the indicated region. Connected cells were those with a visible EPSC detectable across an average of 10 traces. Connected cells in the PFC include those cells that had no visible Li-EPSC until after high frequency stimulation. **(b)** Percent change in Li-EPSCs amplitude during the first five pulses of a 20 Hz train of light pulses activating PFC or PPTg inputs relative to the first pulse (Two-way RM ANOVA, $F_{(4,60)}$=3.280, P=0.0178, Bonferroni multiple comparisons *P<0.05, ***P<0.001; PFC n=8 cells, PPTg n=9 cells). **(c)** Percent change in amplitude of Li-EPSCs before and after high frequency stimulation of PFC or PPTg inputs relative to pre-stimulus train amplitude. PFC inputs were stimulated in the presence or absence of AP5 (100μM), which remained in the bath for the duration of the

experiment. (Two-way RM ANOVA, $F_{(14,154)}$=2.40, P=0.0046, Bonferroni multiple comparisons vs PPTg *P<0.05, **P<0.01; PFC n=8 cells, PFC+AP5 = 7 cells, PPTg n=9 cells). **(d)** Percent of baseline Li-EPSC amplitude following 3× 1s stimulus trains at the indicated frequencies (One-way RM ANOVA, $F_{(3,8)}$=13.13, P<0.0001, Tukey's Multiple Comparisons ***P<0.001 vs Pre, n=9 cells). **(e)** Numbers of connected and not connected Vgat- and Vgat+ cells patched in the VTA with ChR2 expressed in the indicated region. Connected cells were those with a visible IPSC detectable across an average of 10 traces. Error bars represent s.e.m.

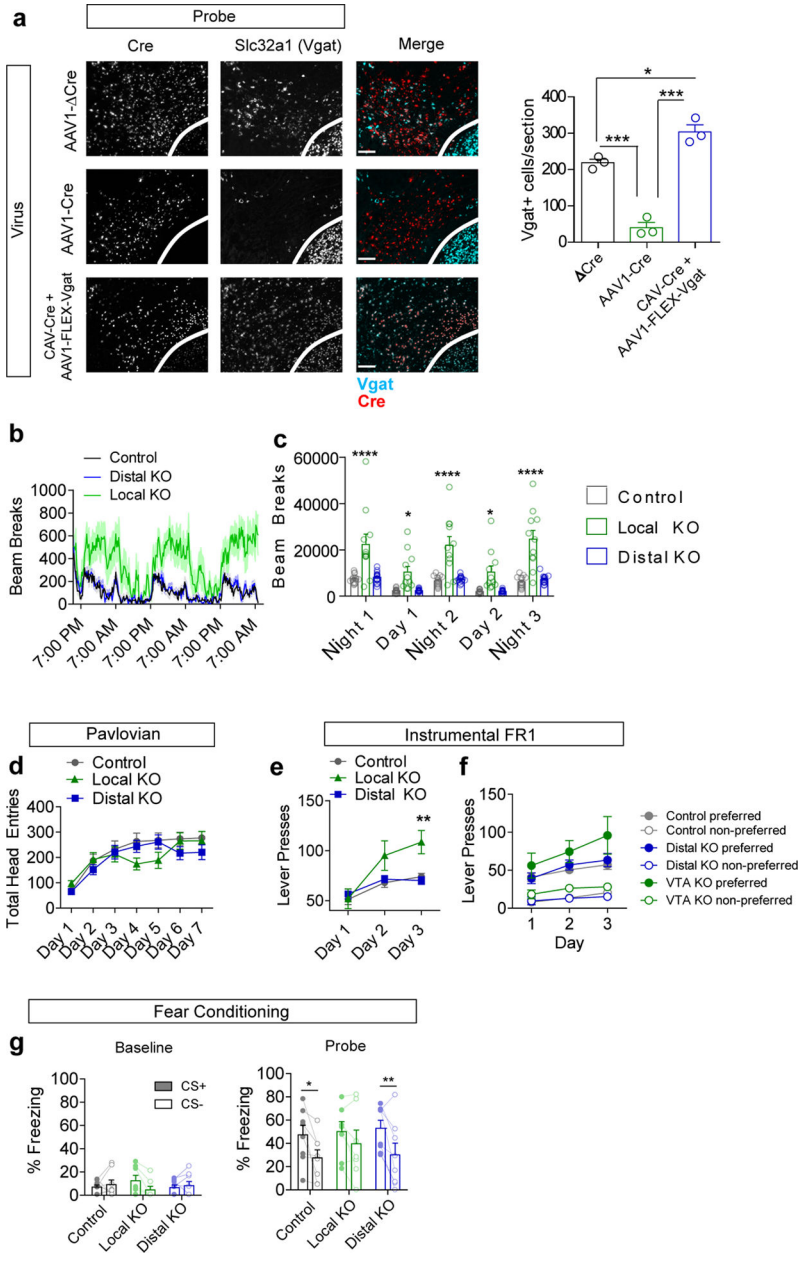


**Extended Data Fig. 6. Local and distal Vgat knockout**

**(a)** Example images of RNAscope *in situ* labeling *Cre* and *Slc32a1* (Vgat) in the VTA following injection of indicated viruses (red=Cre, cyan=Vgat), and quantification of Vgat+ cells/section (n=3 mice/group, One way ANOVA $F_{(2,6)}$=77.97 p<0.0001, Tukey's multiple comparisons *p<0.05, ***p<0.001, scale bar = 100 μm). **(b)** Locomotor activity (measured as infrared beam breaks) measured in 15 min bins (line) with s.e.m. (shading). **(c)** Locomotor activity summed over three nights (7 pm to 7 am) and two days (7 am to 7 pm) (Control n=13 mice, VTA KO n=11, Distal KO n=15; Two-way RM ANOVA $F_{(8,144)}$=6.33, p<0.0001; Bonferroni multiple comparisons *p<0.05, ****p<0.0001). **(d)** Total head entries during each day of Pavlovian training (n=23 mice/group control, 21 VTA KO, 27 distal KO; 2-way RM ANOVA $F_{(12,402)}$=1.9, p=0.032; Bonferroni multiple comparisons did not achieve significance). **(e)** Total lever presses during each day of FR1 instrumental conditioning (1 hour session/day) (Control n=21 mice, VTA KO n=14 mice, Distal KO n=27 mice; Two-way RM ANOVA $F_{(4,118)}$=5.35, p=0.0005; Bonferroni multiple comparisons **p<0.01). **(f)** Lever presses on the preferred and non-preferred levers during 3 days of FR1 instrumental conditioning (Control n=15 mice, VTA KO n=11 mice, Distal KO n=15 mice). **(g)** Percent of time spent freezing during delivery of the CS+ or CS− tone during a baseline pretest or following two days of fear conditioning (n=8 for Control and Distal KO, n=7 for Local KO; Probe: 2-way RM ANOVA significant effect of CS $F_{(1,20)}$=19.79 p=0.0002, Bonferroni multiple comparisons *p<0.05, **p<0.01). Error bars represent s.e.m.

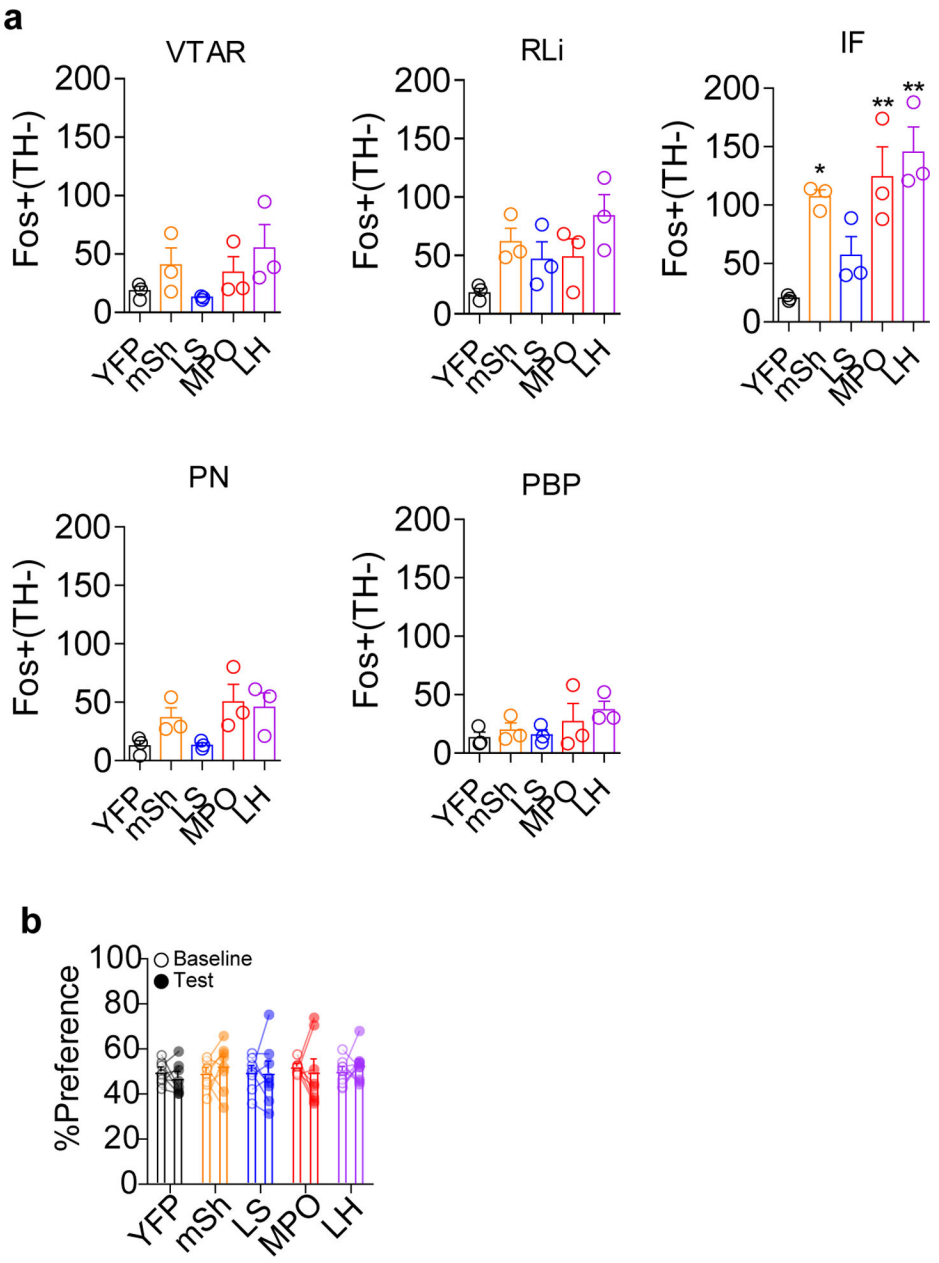


**Extended Data Fig. 7. Fos induction in TH− cells and Jaws RTPA**

**(a)** Number of Fos+ TH− cells in each VTA subregion in Vgat-Cre mice expressing YFP or ChR2-YFP in the indicated brain region. (n=3 mice/group, For IF: One-way ANOVA $F_{(4,10)}$=9.207, p=0.002; *p<0.05, **p<0.01 vs. YFP.) **(b)** Real-time place aversion assay comparing percent of time spent in the light paired chamber during the pretest (baseline) period and during the light stimulation period for Vgat-Cre mice expressing YFP or Jaws-GFP in the indicated regions (n=8 for all groups except n=10 for LH). Error bars represent s.e.m.

## Supplementary Material

Refer to Web version on PubMed Central for supplementary material.

## Acknowledgments

We thank members of the Zweifel lab for scientific discussion on the design and implementation of experiments. We also thank Dr. James Allen for assistance in the production of AAV viral vectors. This work was funded by the US National Institutes of Health (P50MH10642, R01-MH104450 and R01-DA044315 L.S.Z).

## References

1. Morales M & Margolis EB Ventral tegmental area: cellular heterogeneity, connectivity and behaviour. Nature reviews. Neuroscience 18, 73–85, doi:10.1038/nrn.2016.165 (2017). [PubMed: 28053327]
2. Jhou TC, Fields HL, Baxter MG, Saper CB & Holland PC The rostromedial tegmental nucleus (RMTg), a GABAergic afferent to midbrain dopamine neurons, encodes aversive stimuli and inhibits motor responses. Neuron 61, 786–800, doi:10.1016/j.neuron.2009.02.001 (2009). [PubMed: 19285474]
3. Kaufling J, Veinante P, Pawlowski SA, Freund-Mercier MJ & Barrot M Afferents to the GABAergic tail of the ventral tegmental area in the rat. The Journal of comparative neurology 513, 597–621, doi:10.1002/cne.21983 (2009). [PubMed: 19235223]
4. Brown MT et al. Ventral tegmental area GABA projections pause accumbal cholinergic interneurons to enhance associative learning. Nature 492, 452–456, doi:10.1038/nature11657 (2012). [PubMed: 23178810]
5. Cohen JY, Haesler S, Vong L, Lowell BB & Uchida N Neuron-type-specific signals for reward and punishment in the ventral tegmental area. Nature 482, 85–88, doi:10.1038/nature10754 (2012). [PubMed: 22258508]
6. Yoo JH et al. Ventral tegmental area glutamate neurons co-release GABA and promote positive reinforcement. Nature communications 7, 13697, doi:10.1038/ncomms13697 (2016).
7. Qi J et al. VTA glutamatergic inputs to nucleus accumbens drive aversion by acting on GABAergic interneurons. Nature neuroscience 19, 725–733, doi:10.1038/nn.4281 (2016). [PubMed: 27019014]
8. Beier KT et al. Circuit Architecture of VTA Dopamine Neurons Revealed by Systematic Input-Output Mapping. Cell 162, 622–634, doi:10.1016/j.cell.2015.07.015 (2015). [PubMed: 26232228]
9. Lammel S et al. Input-specific control of reward and aversion in the ventral tegmental area. Nature 491, 212–217, doi:10.1038/nature11527 (2012). [PubMed: 23064228]
10. Menegas W et al. Dopamine neurons projecting to the posterior striatum form an anatomically distinct subclass. eLife 4, e10032, doi:10.7554/eLife.10032 (2015). [PubMed: 26322384]
11. Yang H et al. Nucleus Accumbens Subnuclei Regulate Motivated Behavior via Direct Inhibition and Disinhibition of VTA Dopamine Subpopulations. Neuron 97, 434–449 e434, doi:10.1016/j.neuron.2017.12.022 (2018). [PubMed: 29307710]
12. Watabe-Uchida M, Zhu L, Ogawa SK, Vamanrao A & Uchida N Whole-brain mapping of direct inputs to midbrain dopamine neurons. Neuron 74, 858–873, doi:10.1016/j.neuron.2012.03.017 (2012). [PubMed: 22681690]
13. Faget L et al. Afferent Inputs to Neurotransmitter-Defined Cell Types in the Ventral Tegmental Area. Cell reports 15, 2796–2808, doi:10.1016/j.celrep.2016.05.057 (2016). [PubMed: 27292633]
14. Sesack SR & Grace AA Cortico-Basal Ganglia reward network: microcircuitry. Neuropsychopharmacology : official publication of the American College of Neuropsychopharmacology 35, 27–47, doi:10.1038/npp.2009.93 (2010). [PubMed: 19675534]
15. Geisler S, Derst C, Veh RW & Zahm DS Glutamatergic afferents of the ventral tegmental area in the rat. J Neurosci 27, 5730–5743, doi:10.1523/JNEUROSCI.0012-07.2007 (2007). [PubMed: 17522317]

16. Rinvik E & Grofova I Observations on the fine structure of the substantia nigra in the cat. Experimental brain research. Experimentelle Hirnforschung. Experimentation cerebrale 11, 229–248 (1970). [PubMed: 4320004]
17. Chung AS, Miller SM, Sun Y, Xu X & Zweifel LS Sexual congruency in the connectome and translatome of VTA dopamine neurons. Scientific reports 7, 11120, doi:10.1038/s41598-017-11478-5 (2017). [PubMed: 28894175]
18. Gore BB et al. Roundabout receptor 2 maintains inhibitory control of the adult midbrain. eLife 6, doi:10.7554/eLife.23858 (2017).
19. Jennings JH et al. Distinct extended amygdala circuits for divergent motivational states. Nature 496, 224–228, doi:10.1038/nature12041 (2013). [PubMed: 23515155]
20. Nieh EH et al. Inhibitory Input from the Lateral Hypothalamus to the Ventral Tegmental Area Disinhibits Dopamine Neurons and Promotes Behavioral Activation. Neuron 90, 1286–1298, doi:10.1016/j.neuron.2016.04.035 (2016). [PubMed: 27238864]
21. McHenry JA et al. Hormonal gain control of a medial preoptic area social reward circuit. Nature neuroscience 20, 449–458, doi:10.1038/nn.4487 (2017). [PubMed: 28135243]
22. Hjelmstad GO, Xia Y, Margolis EB & Fields HL Opioid modulation of ventral pallidal afferents to ventral tegmental area neurons. The Journal of neuroscience : the official journal of the Society for Neuroscience 33, 6454–6459, doi:10.1523/JNEUROSCI.0178-13.2013 (2013). [PubMed: 23575843]
23. Bocklisch C et al. Cocaine disinhibits dopamine neurons by potentiation of GABA transmission in the ventral tegmental area. Science 341, 1521–1525, doi:10.1126/science.1237059 (2013). [PubMed: 24072923]
24. Sanford CA et al. A Central Amygdala CRF Circuit Facilitates Learning about Weak Threats. Neuron 93, 164–178, doi:10.1016/j.neuron.2016.11.034 (2017). [PubMed: 28017470]
25. Paxinos G, Franklin KBJ & Franklin KBJ The mouse brain in stereotaxic coordinates. 2nd edn, (Academic Press, 2001).
26. Tan KR et al. GABA neurons of the VTA drive conditioned place aversion. Neuron 73, 1173–1183, doi:10.1016/j.neuron.2012.02.015 (2012). [PubMed: 22445344]
27. Dobi A, Margolis EB, Wang HL, Harvey BK & Morales M Glutamatergic and nonglutamatergic neurons of the ventral tegmental area establish local synaptic contacts with dopaminergic and nondopaminergic neurons. The Journal of neuroscience : the official journal of the Society for Neuroscience 30, 218–229, doi:10.1523/JNEUROSCI.3884-09.2010 (2010). [PubMed: 20053904]
28. Xiao C et al. Cholinergic Mesopontine Signals Govern Locomotion and Reward through Dissociable Midbrain Pathways. Neuron 90, 333–347, doi:10.1016/j.neuron.2016.03.028 (2016). [PubMed: 27100197]
29. Qi J et al. A glutamatergic reward input from the dorsal raphe to ventral tegmental area dopamine neurons. Nature communications 5, 5390, doi:10.1038/ncomms6390 (2014).
30. Liu Z et al. Dorsal Raphe Neurons Signal Reward through 5-HT and Glutamate. Neuron 81, 1360–1374, doi:10.1016/j.neuron.2014.02.010 (2014). [PubMed: 24656254]
31. Poulin JF et al. Mapping projections of molecularly defined dopamine neuron subtypes using intersectional genetic approaches. Nature neuroscience, doi:10.1038/s41593-018-0203-4 (2018).
32. Tritsch NX, Ding JB & Sabatini BL Dopaminergic neurons inhibit striatal output through non-canonical release of GABA. Nature 490, 262–266, doi:10.1038/nature11466 (2012). [PubMed: 23034651]
33. Edwards NJ et al. Circuit specificity in the inhibitory architecture of the VTA regulates cocaine-induced behavior. Nature neuroscience 20, 438–448, doi:10.1038/nn.4482 (2017). [PubMed: 28114294]
34. Liu QS, Pu L & Poo MM Repeated cocaine exposure in vivo facilitates LTP induction in midbrain dopamine neurons. Nature 437, 1027–1031, doi:10.1038/nature04050 (2005). [PubMed: 16222299]
35. Jo YS, Heymann G & Zweifel LS Dopamine Neurons Reflect the Uncertainty in Fear Generalization. Neuron 100, 916–925 e913, doi:10.1016/j.neuron.2018.09.028 (2018). [PubMed: 30318411]

36. Burkett JP & Young LJ The behavioral, anatomical and pharmacological parallels between social attachment, love and addiction. Psychopharmacology (Berl) 224, 1–26, doi:10.1007/s00213-012-2794-x (2012). [PubMed: 22885871]
37. Barbano MF, Wang HL, Morales M & Wise RA Feeding and Reward Are Differentially Induced by Activating GABAergic Lateral Hypothalamic Projections to VTA. The Journal of neuroscience : the official journal of the Society for Neuroscience 36, 2975–2985, doi:10.1523/JNEUROSCI.3799-15.2016 (2016). [PubMed: 26961951]
38. Chuong AS et al. Noninvasive optical inhibition with a red-shifted microbial rhodopsin. Nature neuroscience 17, 1123–1129, doi:10.1038/nn.3752 (2014). [PubMed: 24997763]
39. Tian J et al. Distributed and Mixed Information in Monosynaptic Inputs to Dopamine Neurons. Neuron 91, 1374–1389, doi:10.1016/j.neuron.2016.08.018 (2016). [PubMed: 27618675]
40. Berke JD What does dopamine mean? Nature neuroscience 21, 787–793, doi:10.1038/s41593-018-0152-y (2018). [PubMed: 29760524]
41. Mameli-Engvall M et al. Hierarchical control of dopamine neuron-firing patterns by nicotinic receptors. Neuron 50, 911–921, doi:10.1016/j.neuron.2006.05.007 (2006). [PubMed: 16772172]
42. Paladini CA & Tepper JM GABA(A) and GABA(B) antagonists differentially affect the firing pattern of substantia nigra dopaminergic neurons in vivo. Synapse 32, 165–176, doi:10.1002/(SICI)1098-2396(19990601)32:3<165::AID-SYN3>3.0.CO;2-N (1999). [PubMed: 10340627]
43. Faget L et al. Opponent control of behavioral reinforcement by inhibitory and excitatory projections from the ventral pallidum. Nature communications 9, 849, doi:10.1038/s41467-018-03125-y (2018).
44. Parker JG et al. Absence of NMDA receptors in dopamine neurons attenuates dopamine release but not conditioned approach during Pavlovian conditioning. Proceedings of the National Academy of Sciences of the United States of America 107, 13491–13496, doi:10.1073/pnas.1007827107 (2010). [PubMed: 20616081]
45. Nieh EH et al. Decoding neural circuits that control compulsive sucrose seeking. Cell 160, 528–541, doi:10.1016/j.cell.2015.01.003 (2015). [PubMed: 25635460]
46. Heymann G et al. Synergy of Distinct Dopamine Projection Populations in Behavioral Reinforcement. Neuron 105, 909–920 e905, doi:10.1016/j.neuron.2019.11.024 (2020). [PubMed: 31879163]
47. Gunaydin LA et al. Natural neural projection dynamics underlying social behavior. Cell 157, 1535–1551, doi:10.1016/j.cell.2014.05.017 (2014). [PubMed: 24949967]
48. Vega-Quiroga I, Yarur HE & Gysling K Lateral septum stimulation disinhibits dopaminergic neurons in the antero-ventral region of the ventral tegmental area: Role of GABA-A alpha 1 receptors. Neuropharmacology 128, 76–85, doi:10.1016/j.neuropharm.2017.09.034 (2018). [PubMed: 28963038]
49. Parker JG, Beutler LR & Palmiter RD The contribution of NMDA receptor signaling in the corticobasal ganglia reward network to appetitive Pavlovian learning. The Journal of neuroscience : the official journal of the Society for Neuroscience 31, 11362–11369, doi:10.1523/JNEUROSCI.2411-11.2011 (2011). [PubMed: 21813695]
50. Ting JT, Daigle TL, Chen Q & Feng G Acute brain slice methods for adult and aging animals: application of targeted patch clamp analysis and optogenetics. Methods Mol Biol 1183, 221–242, doi:10.1007/978-1-4939-1096-0_14 (2014). [PubMed: 25023312]

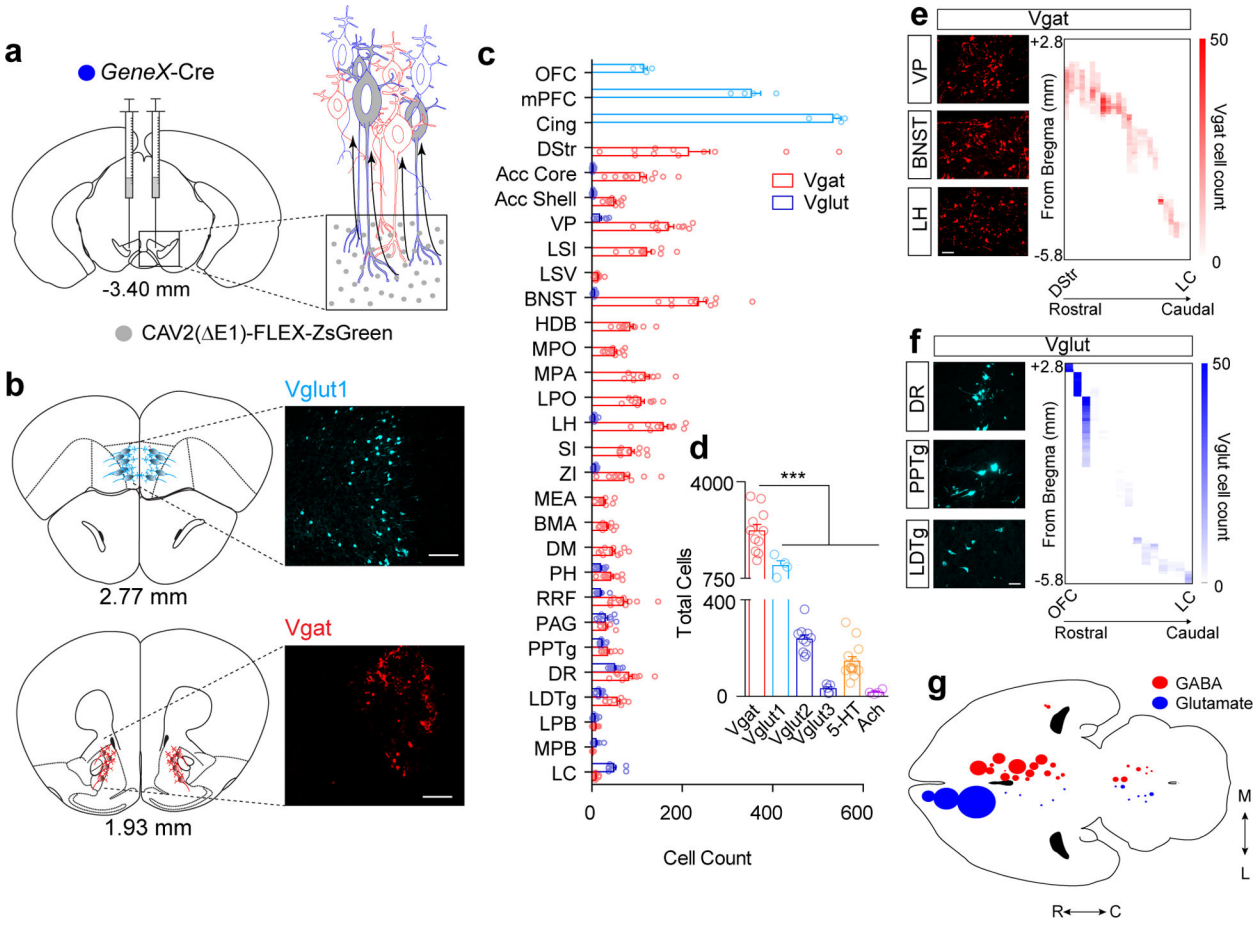


**Figure 1. Retrograde mapping of neurotransmitter-specific inputs to the VTA.**

**(a)** Illustration of CAV2-FLEX-ZsGreen injection into the VTA (gray circles) and retrograde transport. Note: all cells projecting to the VTA can take up the CAV2 virus, but only neurons of a designated cell type based on Cre expression can turn on ZsGreen expression (gray cells). **(b)** Atlas illustrations and example images of ZsGreen-labeled cells (Vglut1-expressing, light blue; Vgat-expressing red, Scale bar 100μm). **(c)** Cell counts normalized to the total number of labeled neurons per mouse in identified brain regions from Vgat (red) or Vglut (blue) Cre-driver lines (Vgat n=11 mice, Vglut1 n=4; Vglut2 n=10; Vglut3 n=5). **(d)** Total cell counts across the entire brain for each neurotransmitter phenotype (Vgat n=11 mice, Vglut1 n=4; Vglut2 n=10; Vglut3 n=5, 5-HT n=13, Ach n=4; One-way ANOVA $F_{(5, 41)}$=60.62 p<0.0001, ***p<0.001 Tukey's multiple comparisons). **(e-f)** Representative images of retrogradely labeled Vgat (a) and Vglut (b) cells in indicated regions, (Scale bars 50 μm) and heatmaps illustrating cell counts along the rostral-caudal axis (y-axis) in each region (x-axis). **(g)** Cell density map illustrating relative number and location of projection neurons. Error bars represent s.e.m. List of abbreviations: OFC: orbitofrontal cortex, mPFC: medial prefrontal cortex, Cingulate: cingulate cortex, DStr: dorsal striatum, NAc Core: nucleus accumbens core, NAc Shell: nucleus accumbens shell, LSI: lateral septum intermediate, LSV: lateral septum ventral, VP: ventral pallidum, HDB/VDB: horizontal diagonal band/vertical diagonal band, BNST: bed nucleus of the stria terminalis, MPO: medial preoptic nucleus, MPA: medial preoptic area, LPO: lateral preoptic area, SI:

substantia inominata, ZI: zona incerta, LH: lateral hypothalamic area, PH: posterior hypothalamic area, BMA: basomedial amygdala, MEA: medial amygdala, DM: dorsomedial hypothalamic nucleus, VTA: ventral tegmental area, RRF: retrorubral field, PAG: periaquiductal gray, DR: dorsal raphe nulceus, PPTg: pedunculopontine tegmental nucleus, LDTg: laterodorsal tegmental nucleus, LPB: lateral parabrachial nucleus, MPB: medial parabrachial nucleus, LC: locus coeruleus.

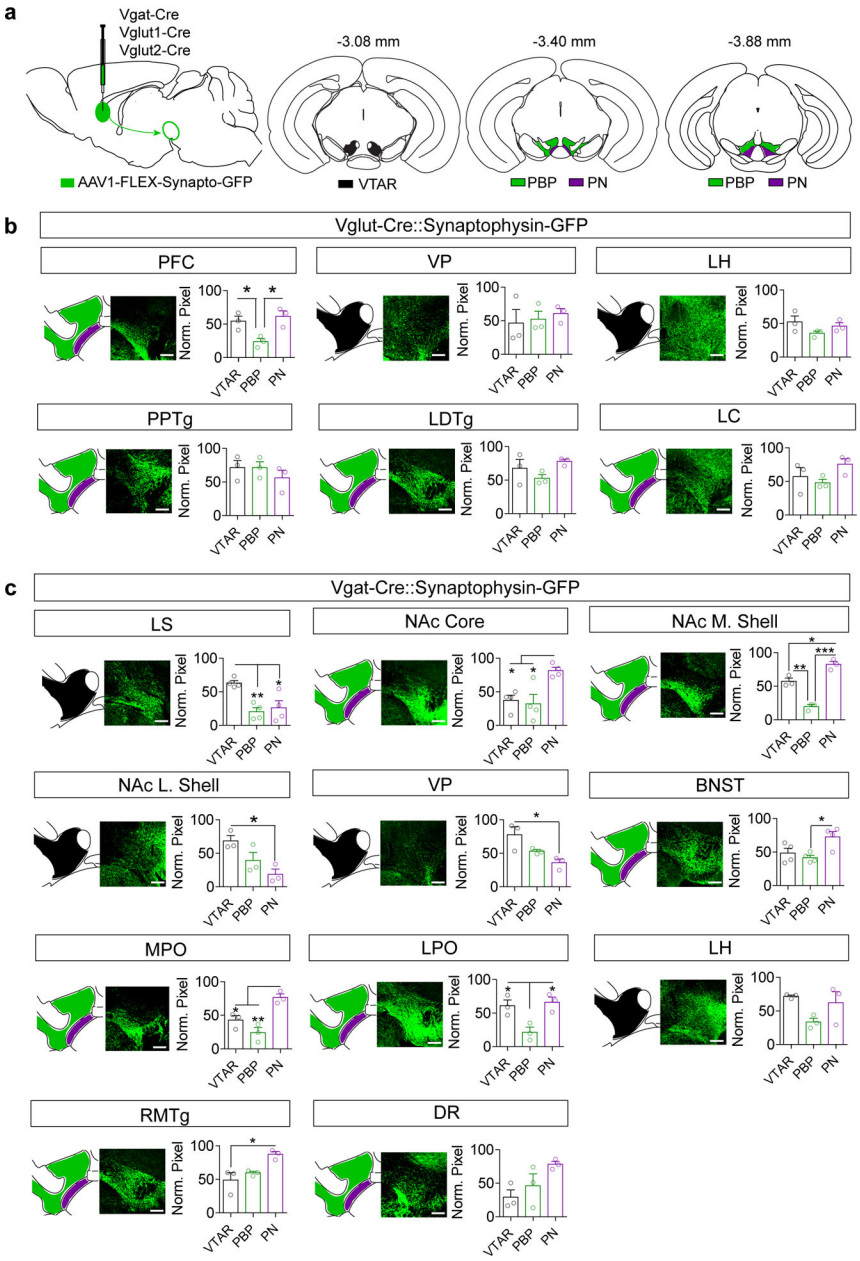


**Figure 2. Glutamatergic and GABAergic innervation of VTA subregions.**

**(a)** Illustration of AAV1-FLEX-synaptophysinGFP injection into various Cre lines, and atlas images of the VTA showing designated rostral (VTAR), parabrachial pigmented nucleus (PBP), and paranigral (PN) subdivisions, with indicated distance from bregma. **(b)** Representative images and quantification of synaptophysinGFP projections in Vglut1 mice (PFC) or Vglut2 mice (all other regions) to the subdivisions of the VTA expressed as normalized pixel densities relative to the peak area of innervation (n=3 mice/group; data measured from 9 VTA sections/mouse. One-way ANOVA: PFC: $F_{(2,6)}$=8.34, p=0.019, *P<0.05 Tukey's multiple comparisons). **(c)** Representative images and quantification of synaptophysinGFP projections in Vgat mice to the subdivisions of the VTA expressed as normalized pixel densities relative to the peak area of innervation (n=3 mice/group, 9

sections/mouse for all regions except n=4 mice for LS, NAc core, and BNST. One-way ANOVA: LS: $F_{(2,9)}$=10.08, p=0.005, NAc Core: $F_{(2,9)}$=8.17, p=0.01, NAc M. Shell: $F_{(2,6)}$=57.87, p=0.0001, NAc L. Shell: $F_{(2,6)}$=7.02, p=0.026, VP: $F_{(2,6)}$=7.24, p=0.025, BNST: $F_{(2,9)}$=6.328, p=0.019, MPO: $F_{(2,6)}$=16.16, p=0.004, LPO: $F_{(2,6)}$=9.35, p=0.014, LH: $F_{(2,6)}$=4.162, p=0.085, RMTg: $F_{(2,6)}$=8.34, p=0.019, DR: $F_{(2,9)}$=4.162, p=0.074; *p<0.05, **p<0.01, ***p<0.001 Tukey's multiple comparisons). Error bars represent s.e.m. Scale bar = 200 μm.

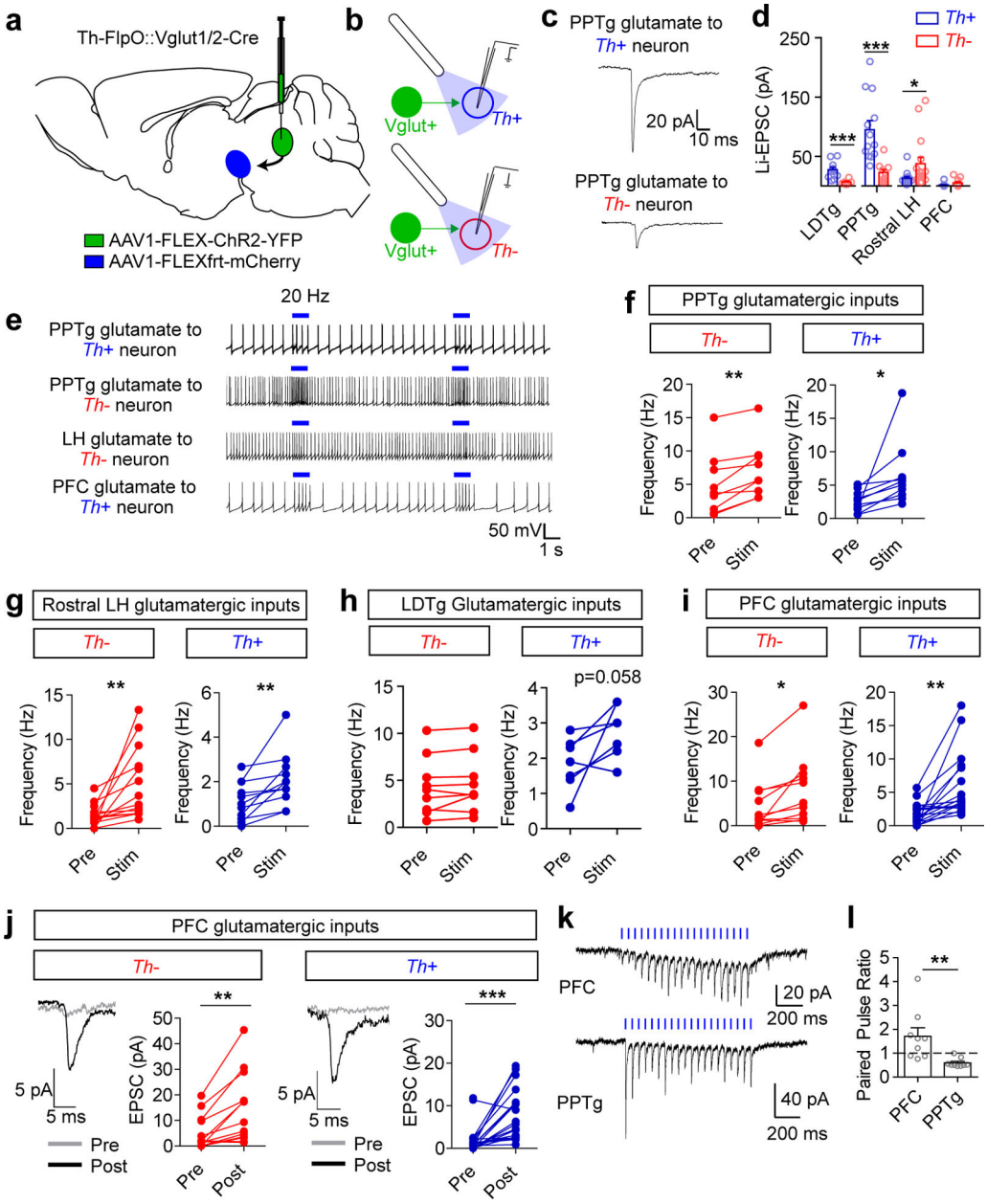


**Figure 3. Connectivity of glutamatergic inputs to the VTA.**

**(a)** Illustration of AAV1-FLEX-ChR2-YFP injection into the region of interest and AAV1-FLEXfrt-mCherry injection into the VTA in Th-FlpO::Vglut Cre mice. **(b)** Illustration of patch-clamp recordings from *Th+* (dopamine) and *Th−* (non-dopamine) VTA neurons and blue light stimulation of ChR2 inputs. **(c)** Example traces (average of 10 sweeps) and **(d)** quantification of light-evoked EPSCs (Li-EPSCs) recorded from *Th+* and *Th−* neurons in the VTA, identified by fluorescence. Only cells with a measurable connection are included here; for PFC, amplitudes are measured prior to 20 Hz stimulation (see below). See Extended Data Fig. 5 for numbers of connected vs. unconnected cells for each input. (LDTg *Th+* n=11 cells, *Th−* n=6; PPTg *Th+* n=13, *Th−* n=10; LH *Th+* n=14, *Th−* n=16; PFC *Th+* n=23, *Th−* n=18. Student's two-tailed t testLDTg: p=0.004, PPTg: p=0.001, LH: p=0.045.)

**(e)** Example traces of action potential firing; blue bar indicates 1 second of 20 Hz light stimulus. **(f-i)** Quantification of action potential frequency before and during 20 Hz light stimulation, averaged from 3 sweeps/cell. (PPTg *Th*− n=9 cells, *Th+* n=10; LDTg *Th*− n=9, *Th+* n=7; LH *Th*− n=14, *Th+* n=12; PFC *Th*− n=11; *Th+* n=18; Paired two-tailed t tests PPTg TH−: p=0.003, PPTg TH+: p=0.034, LH TH−: p=0.005, LH TH+: p=0.005, PFC TH−: p=0.011, PFC TH+: p=0.001). **(j)** Example traces (average of 10 sweeps) and Li-EPSC amplitudes recorded before and after 5× 1 second 20 Hz light stimulation. (*Th*− n=13 cells, *Th+* n=23 cells, paired two-tailed t tests TH−: p=0.002, TH+: p=0.0002). **(k)** Example traces of Li-EPSCs from PFC and PPTg inputs evoked by 20 Hz light stimulus. **(l)** Paired pulse ratio (second pulse amplitude/first pulse amplitude) of Li-EPSCs from PFC and PPTg inputs (n=9 cells/group, Student's two-tailed t test p=0.007). For all panels error bars represent s.e.m.

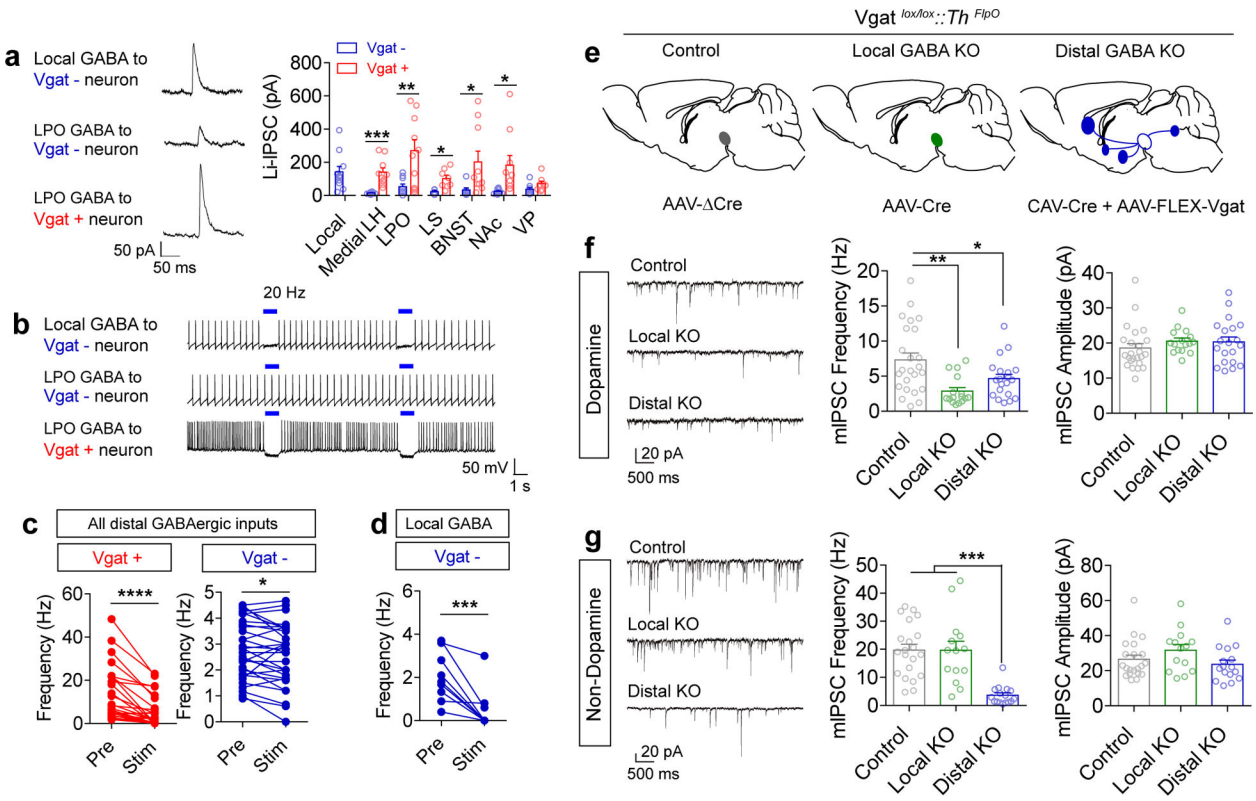


**Figure 4. Connectivity of GABAergic inputs to the VTA.**

**(a)** Example traces (average of 10 sweeps) and quantification of light-evoked IPSCs (Li-IPSCs) recorded from Vgat- and Vgat+ neurons in the VTA, identified by fluorescence. Only cells with a measureable connection are included here; see Extended Data Fig. 5 for numbers of connected vs. unconnected cells for each input (local n=11 cells; LH Vgat- n=8, Vgat+ n=10; LPO Vgat- n=10, Vgat+ n=10; LS Vgat- n=5, Vgat+ n=8; BNST Vgat- n=8, Vgat+ n=10, NAc Vgat- n=10, Vgat+ n=10; VP Vgat- n=9, Vgat+ n=8; Student's two-tailed t test LH: p=0.0004, LPO: p=0.005, LS: p=0.011, BNST: p=0.036, NAc: p=0.016). **(b)** Example traces of action potential firing; blue bar indicates 1 second of 20 Hz light stimulus. **(c-d)** Quantification of action potential frequency before and during 20 Hz light stimulation, averaged from 3 sweeps/cell (Distal Vgat+ n=28 cells; Distal Vgat- n=33; Local n=10; paired two-tailed t tests distal Vgat+: p<0.0001, distal Vgat-: p=0.017, local Vgat-: p=0.0007). **(e)** Illustration of experimental groups. Vgat$^{lox/lox}$::$Th^{FlpO}$ mice were injected in the VTA with the indicated virus(es) mixed with AAV1-FLEXfrt-mCherry to label dopamine neurons for slice recording. **(f-g)** Example traces and quantification of mIPSC frequency and amplitude recorded from *Th+* (dopamine; f) and *Th−* (non-dopamine; g) neurons (Dopamine: n=24 cells control, 16 VTA KO, 20 distal KO; Non-dopamine: 21 cells control, 14 cells VTA KO, 16 cells distal KO. One-way ANOVA: Dopamine frequency $F_{(2,57)}$=7.48, p=0.001, Non-dopamine frequency $F_{(2,48)}$=17.31, p<0.0001; *p<0.05, **p<0.01, ***p<0.001 Tukey's multiple comparisons). Error bars represent s.e.m.

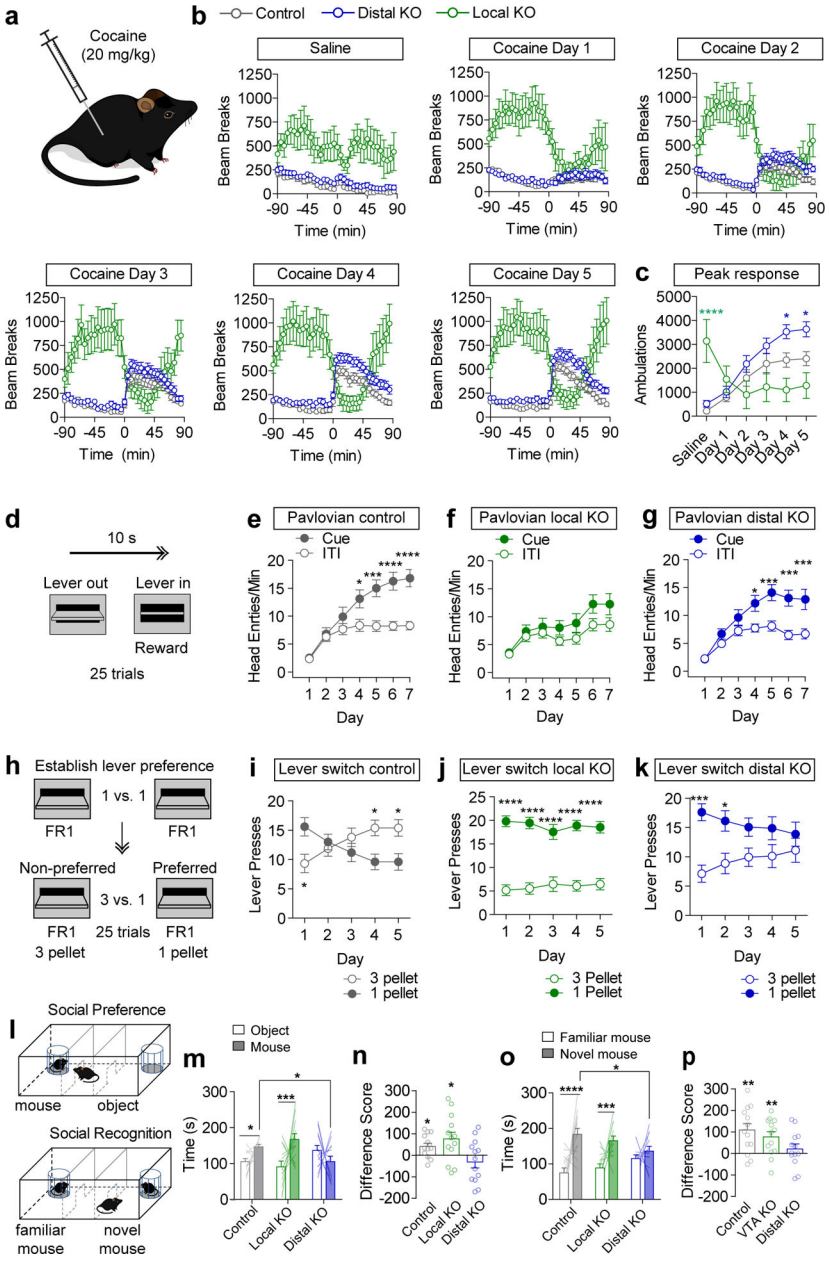


**Figure 5. Vgat knockout from local and distal sources differentially affects reward behaviors.**

**(a)** Mice received saline or cocaine injections (subcutaneous, 20 mg/kg). **(b)** Locomotor activity, measured as infrared beam breaks, before and after saline or cocaine injection at time zero (Control n=16 mice, Distal KO n=18, VTA KO n=10). **(c)** Peak locomotor response, summed from 15–45 min post injection. (Control n=16 mice, Distal KO n=18, VTA KO n=10; Two-way RM ANOVA, Distal KO vs. Control, effect of virus $F_{(1,32)}$=6.05, p=0.02; VTA KO vs. Control, Interaction $F_{(5,115)}$=13.58, p<0.0001, Bonferroni multiple comparisons *p<0.05, ****p<0.0001.) **(d)** Schematic of Pavlovian conditioning with lever extension for 10s serving as a compound visual/auditory cue, and lever retraction coinciding with reward delivery. **(e-g)** Average head entries/minute during the cue or the inter-trial interval (ITI) period on each day of Pavlovian conditioning (n=23 mice/group control, 21

VTA KO, 27 distal KO. Two-way RM ANOVA: Control Interaction $F_{(6,264)}$=7.16, p<0.0001, Distal KO Interaction $F_{(6,312)}$=4.21, p=0.0004, Bonferroni multiple comparisons *p<0.05, ***p<0.001, ****p<0.0001). **(h)** Schematic of FR1 conditioning (3 days) followed by lever-switching paradigm in which the value of the non-preferred lever increases to 3 pellets while the value of the preferred lever remains the same. **(i-k)** Presses on high and low reward levers over five days of training (n=15 mice/group control, 11 VTA KO, 15 distal KO. Two-way RM ANOVA: Control Interaction $F_{(4,112)}$=10.96, p<0.0001, VTA KO Effect of Lever $F_{(1,20)}$=73.48, p<0.0001, Distal KO Interaction $F_{(4,112)}$=5.40, p=0.0005, Bonferroni multiple comparisons *p<0.05, ***p<0.001, ****p<0.0001). **(l)** Schematic of social preference and social recognition assay. **(m)** Time spent in the mouse or object chamber during the five minute trial period (n=13 mice/group; Two-way ANOVA Interaction $F_{(2,36)}$=4.56, p=0.017; mouse chamber: distal KO vs. control *p<0.05, Bonferroni selected comparisons between subjects; mouse vs. object: control *p<0.05; local KO ***p<0.001, Fisher's two-tailed single comparison within subjects). **(n)** Difference score (time in mouse chamber – time in object chamber), (Two-tailed one-sample t test, theoretical mean=0, Control: p=0.018, Local KO: p=0.031). **(o)** Time spent in the familiar or novel mouse chamber during the five minute trial period (n=13 mice/group; Two-way ANOVA Interaction $F_{(2,36)}$=5.60, p=0.006; mouse chamber: distal KO vs. control *p<0.05, Bonferroni selected comparisons between subjects; novel mouse vs. familiar mouse: control ****p<0.0001; local KO ***p<0.001, Fisher's two-tailed single comparison within subjects). **(p)** Difference score (time in novel mouse chamber – time in familiar mouse chamber), (Two-tailed one-sample t test, theoretical mean=0, Control: p=0.003, Local KO: p=0.007). Error bars represent s.e.m.

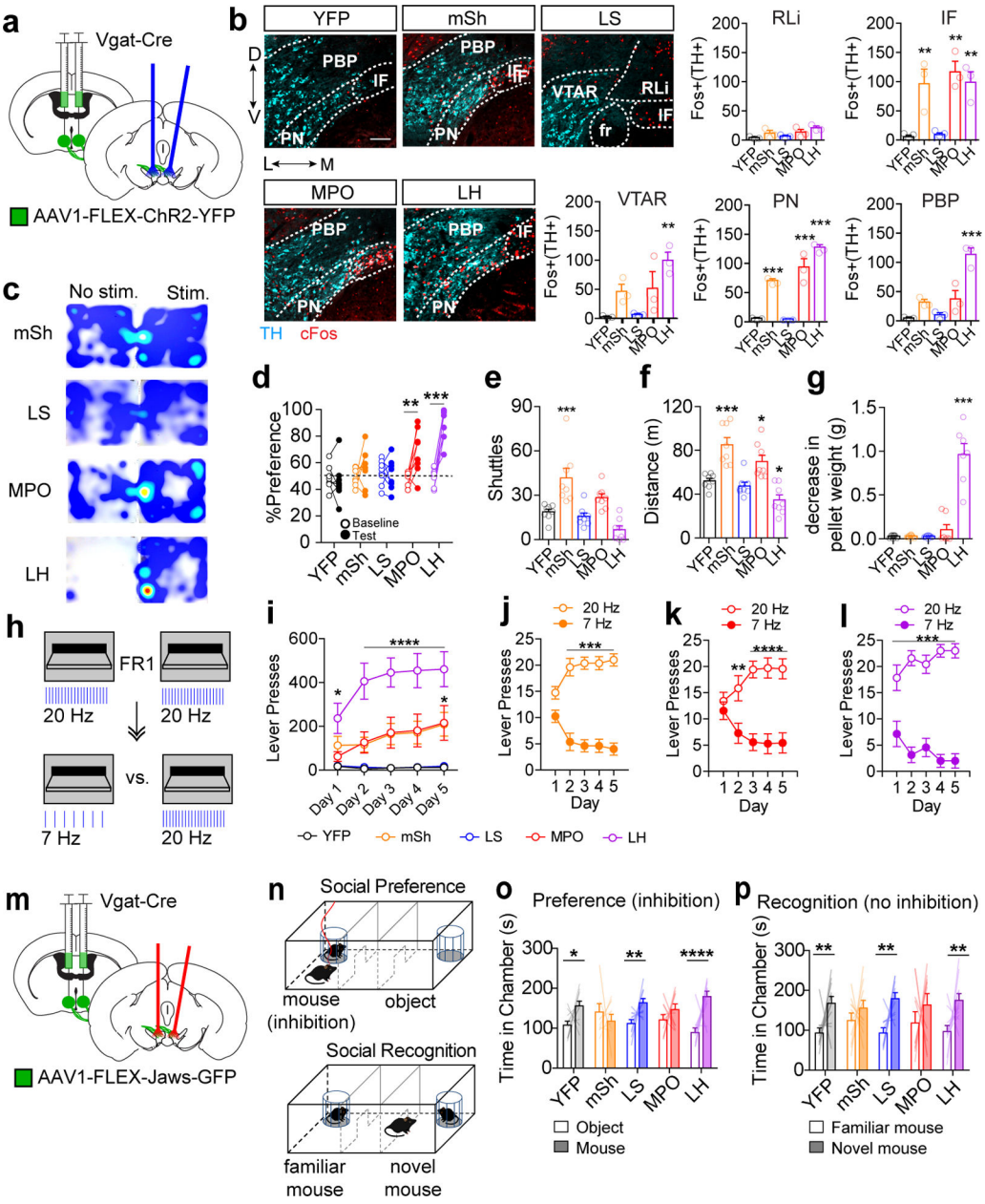


**Figure 6. Optogenetic activation and inhibition of specific distal GABAergic inputs differentially affects dopamine neuron activation and dopamine-dependent behaviors.**

**(a)** Schematic of bilateral ChR2-YFP injection into a Vgat-Cre mouse and bilateral optic fiber implantation above the VTA. **(b)** Example images showing staining for TH (cyan) and cFos (red) in the VTA following 20 Hz light stimulation (scale bar = 100 μm), and quantification of Fos+ TH+ cells in each VTA subregion in Vgat-Cre mice expressing YFP or ChR2-YFP in the indicated brain region (n=3 mice/group, One way ANOVA VTAR:$F_{(4,10)}$=6.644, p=0.007, IF: $F_{(4,10)}$=10.72, p=0.001, PN: $F_{(4,10)}$=62.98, p<0.0001, PBP: $F_{(4,10)}$=25.87, p<0.0001, Dunnett's two-tailed selected comparisons vs. YFP **p<0.01, ***p<0.001). **(c)** Example heat plots showing time spent in No Stim. vs. Stim side of the RTPP arena. **(d)** Percent of time spent in paired chamber during 10 min baseline

pretest or during 20 min light paired session (n=8 mice/group, 2-way RM ANOVA $F_{(4,35)}$=11.56, p<0.0001, Bonferroni multiple comparisons **p<0.01, ***p<0.001). **(e)** Number of shuttles between unpaired and paired chamber during light paired session (n=8 mice/group, One way ANOVA $F_{(4,35)}$=13.69, p<0.0001, Dunnett's two-tailed selected comparisons vs. YFP ***p<0.001). **(f)** Distance traveled during light paired session (n=8 mice/group, One way ANOVA $F_{(4,35)}$=17.47, p<0.0001, Dunnett's two-tailed selected comparisons vs. YFP *p<0.05,***p<0.001).**(g)** Decrease in food pellet weight placed into empty cage with each mouse following 20 min of 20 Hz stim (n=8 mice for YFP and mSh, 7 mice for LS, MPO, and LH; One way ANOVA $F_{(4,32)}$=48.93, p<0.0001, Dunnett's two-tailed selected comparisons vs. YFP ***p<0.001). **(h)** Schematic of lever pressing for light stimulation. Mice received five days of FR1 training in which either lever delivered 20 Hz stimulation, followed by 5 days of training in which their preferred lever was switched to 7 Hz stimulation. **(i)** Number of lever presses per one hour session during 20 Hz acquisition phase (n=8 for YFP, mSh, and LS, n=7 for MPO and LH, 2-way RM ANOVA $F_{(16,132)}$=7.80, p<0.0001, Bonferroni multiple comparisons *p<0.05, ****p<0.0001 vs. YFP). **(j-l)** Lever presses on high or low frequency levers (25 trials) for mSh, MPO, and LH mice (n=8 for mSh, n=7 for MPO and LH; 2-way RM ANOVA mSh $F_{(4,56)}$=17.81 p<0.0001, MPO $F_{(4,48)}$=18.09 p<0.0001, LH $F_{(4,48)}$=6.34 p=0.0004, Bonferroni multiple comparisons **p<0.01, ***p<0.001, ****p<0.0001). **(m)** Schematic of bilateral Jaws-GFP injection into a Vgat-Cre mouse and bilateral optic fiber implantation above the VTA. **(n)** Schematic of social preference and social recognition assays. Mice received red light stimulation when in the mouse chamber during the preference assay. **(o)** Time spent in the mouse or object chamber during the five-minute trial period (n=11 mice for YFP and LH, n=10 mice for mSh, LS, and MPO, Two-way ANOVA Interaction $F_{(4,94)}$=4.76, p=0.002; mouse vs. object: YFP *p<0.05; LS **p<0.01, LH ****P<0.0001, Fisher's two-tailed single comparisons). **(p)** Time spent in the novel or familiar mouse chamber during the five-minute trial period (n=11 mice for YFP and LH, n=10 mice for mSh, LS, and MPO, Two-way ANOVA Chamber $F_{(1,94)}$=26.99, p<0.0001; novel mouse vs. familiar mouse: YFP **p<0.01; LS **p<0.01, LH **p<0.01, Fisher's two-tailed single comparisons). Error bars represent s.e.m.